CRANFIELD UNIVERSITY

IKER RAIGOSO GOITIA

PASSIVE DEFORMATION OF AIRFOIL SUCTION SURFACE TO MATCH THE EFFECTS OF INCREASING AIRFOIL THICKNESS ON A DOUBLE ELEMENT WING IN GROUND EFFECT

SCHOOL OF AEROSPACE, TRANSPORT AND MANUFACTURING
Advanced Motorsport Engineering

MSc
Academic Year: 2020 - 2021

Supervisor: Dr Verónica Marchante Rodriguez
September 2021

CRANFIELD UNIVERSITY

SCHOOL OF AEROSPACE, TRANSPORT AND MANUFACTURING
Advanced Motorsport Engineering

MSc

Academic Year 2020 - 2021

IKER RAIGOSO GOITIA

PASSIVE DEFORMATION OF AIRFOIL SUCTION SURFACE TO MATCH THE EFFECTS OF INCREASING AIRFOIL THICKNESS ON A DOUBLE ELEMENT WING IN GROUND EFFECT

Supervisor: Dr Verónica Marchante Rodriguez
September 2021

This thesis is submitted in partial fulfilment of the requirements for the degree of Advanced Motorsport Engineering MSc

© Cranfield University 2021. All rights reserved. No part of this publication may be reproduced without the written permission of the copyright owner.

ABSTRACT

An investigation has been conducted to compare the effects of airfoil suction surface passive deformation and increase of airfoil thickness in ground effect. Single airfoil configuration exhibits high sensitivity to the increase of Adverse Pressure Gradient (APG) due to ground effect, being necessary the use of double element wing to achieve required pressure distribution. A Computational Fluid Dynamic (CFD) model is developed based on data from literature which is later used for CFD analysis of created geometries. 2D and 3D CFD analysis show that passive deformation of suction surface match the effects of increasing airfoil thickness within a 1% margin. While 2D analysis exhibit an improvement in downforce and efficiency increasing airfoil thickness, 3D analysis does not. 3D analysis also shows a change in tendency for downforce obtaining higher values than baseline from a thickness increase of 8% maximum thickness / chord (t/c). A structural concept was successfully modelled achieving a deformation close to target, providing 4.6% less downforce and 1% less efficiency.

Keywords:

Aerodynamics, Computational Fluid Dynamics, Fluid Structure Interaction, Airfoil Morphing, Aeroelasticity, Motorsport

ACKNOWLEDGEMENTS

I would like to take this opportunity to express my gratitude to Dr Verónica Marchante Rodriguez for her support during this project, specially at the early stages when working on the objectives and scope of the project together with Dr Kim Blackburn and Mr Clive Temple.

My gratitude is also passed on to Dr Marzio Grasso and Dr Zeeshan Rana for their invaluable contribution to structural and fluid modelling respectively. Their technical feedback was key to the success of the project.

I would like to acknowledge the input of Mr Gerard Torres who recommended me to focus my thesis on aeroelasticity before starting this MSc. The time I spent since that day thinking on it provided me opportunity to come up with a novel airfoil morphing design.

And last but not least, I would like to thank my parents, brother, uncle, family and friends for their continued support throughout my studies so that I could pursue my dreams. Also, to my partner, especially for her support during this year full of challenges and a pandemic.

TABLE OF CONTENTS

LIST OF FIGURES

LIST OF TABLES

LIST OF ABBREVIATIONS

KPI	Key Performance Indicator
FSI	Fluid Structure Interaction
AoA	Angle of Attack
Re	Reynolds Number
APG	Adverse Pressure Gradient
F1	Formula One
LE	Leading Edge
TE	Trailing Edge
BC	Boundary Condition

LIST OF VARIABLES

Cl	Lift Coefficient
Cd	Drag Coefficient
Cp	Pressure Coefficient
c	Airfoil Chord
t/c	Airfoil Maximum Thickness Relative to the Chord
h/c	Airfoil Minimum Ground Clearance Relative to the Chord
-L/D	Aerodynamic Efficiency

1 INTRODUCTION

1.1 Background

Airfoil passive deformation is based on the interaction between the structural and fluid characteristics of the system. This coupled effect is analysed through an aeroelastic study which determines the relationship between structural deformations and change in fluid dynamics, in this case, airfoil suction surface and pressure distribution.

Maximising aeroelasticity effects in high performance cars implies gaining a competitive advantage against your opponents. That competitive advantage is essential, especially in motorsport because of rules restrictions (for example Formula One (F1) [1]), where the smallest advantage could decide the winner of the race. Furthermore, the challenge associated with this thesis project will enhance the knowledge and creativity of the author.

1.2 Literature Review

Lap time reduction in motorsport is dependant of tyres performance. In basic terms, tyre longitudinal and lateral maximum force depends on tyre vertical load which can be divided into gravitational and aerodynamic force. Therefore, increasing downforce, tyre performance is improved and consequently lap time reduced. On the other hand, car top speed and fuel consumption is highly dependent of drag force, as the power of drag to overcome on movement is proportional to the cube of the speed.

Car aerodynamics take advantage of ground proximity to generate more downforce, this is called ground effect. While downforce is generated because of wing circulation, ground act as a mirror. Therefore, when ground clearance decrease, “mirrored wing” generated circulation enhance the “original wing” increasing its circulation, hence, producing more downforce. This concept is important to have in mind while reading 1.2.1 chapter.

1.2.1 Effects of Airfoil Thickness in Lift

Effects of airfoil thickness in lift combined with ground effect geared the creation of this thesis idea. First, according to the research showed by Joseph Katz in his book [2], both airfoil thickness and Reynolds Number (Re) affect airfoil maximum lift as illustrated in Figure 1-1.

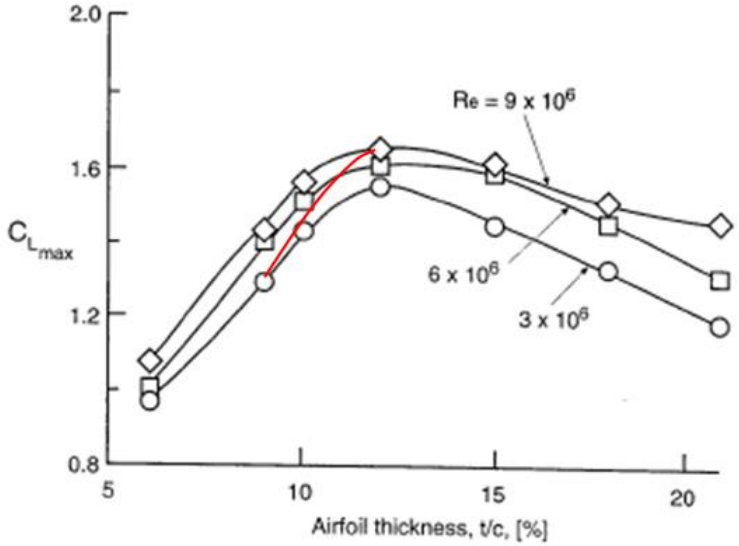

Figure 1-1. Effects of airfoil thickness (t/c) on Cl_{max} (NACA 63) [2]

According to Figure 1-1, there is an optimum thickness for maximum lift, and the higher the Reynolds Number the higher maximum lift (from a higher Angle of Attack (AoA), see Figure 1-2 example) that can be obtained.

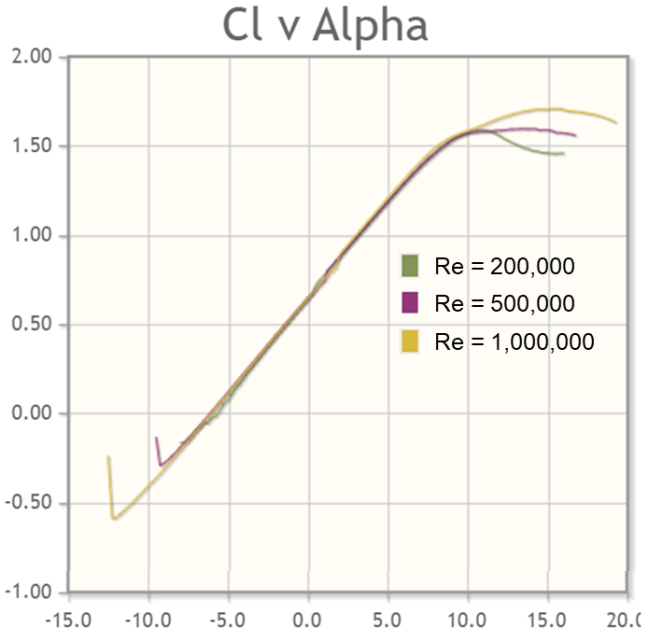

Figure 1-2. NACA 6412 Cl (y-axis) against AoA (x-axis) for different Re [3]

These conclusions led to the following hypothetical situation: single airfoil wing which initial thickness is limited to 9% due to rules dimension boxes. Potential Cl maximum value would increase vertically with the increase of speed (increase of Re), but bigger values could be obtained with higher thickness as speed increase (Figure 1-1, red line).

However, working on maximum lift conditions also means working on low efficiency Figure 1-3 and close to separation. This could lead to hysteresis because of the dynamic stall excited by the pitching motion of the car. Hence this approach has limited real applications. However, if wing thickness is increased when it is close to the ground, it would get advantage of ground effect.

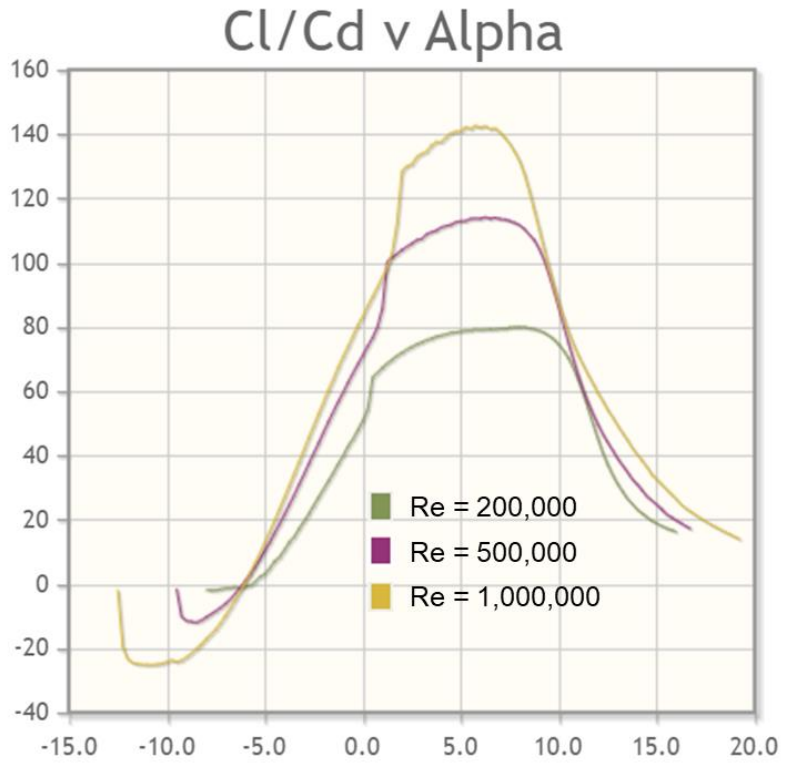

Figure 1-3. NACA 6412 efficiency (Cl/Cd) against AoA for different Re [3]

1.2.2 Experimental Data

Even if simulations are not completely accurate it is important to understand the accuracy of those. For this purpose, experimental data from literature has been used.

1.2.2.1 Single Airfoil in Ground Effect

Investigations have been conducted to analyse the aerodynamic performance of a single airfoil in ground effect. Among different parameters, it has been analysed the impact of ground clearance in the aerodynamic performance.

Based on the literature [4], the downforce generated by the airfoil increases decreasing the ground clearance until it reaches a maximum, from which the performance drops abruptly due to flow separation, see Figure 1-4 (left) and Figure 1-5 (left).

1.2.2.2 Double Element Wing in Ground Effect

This study also measures the pressure distribution in the wing at the centre and the tip of the wing, see Figure 1-5 (right). This information will later be used to understand the accuracy of the CFD model.

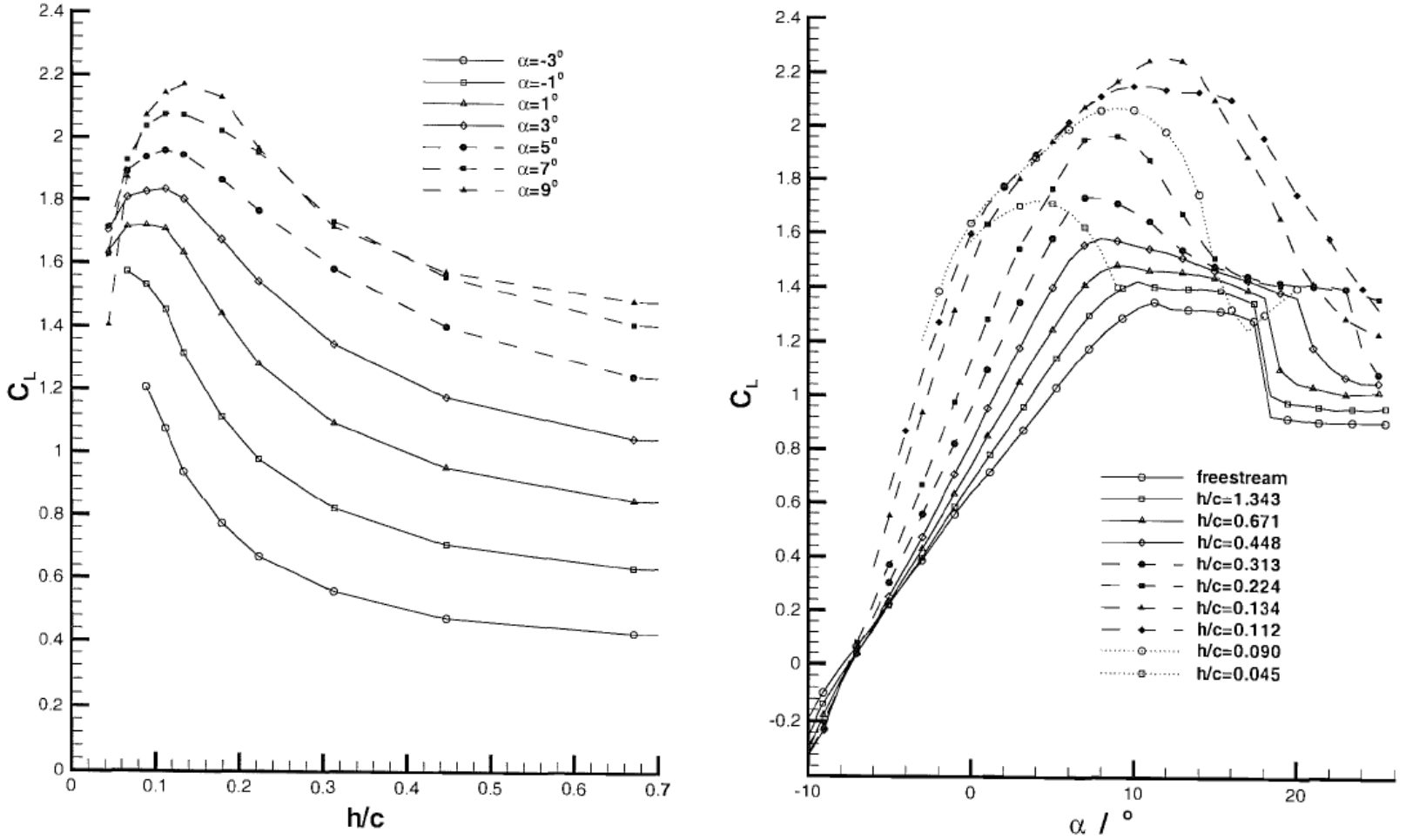

Figure 1-4. Single airfoil in ground effect; Downforce with height for various incidences (left) and lift curves at different heights (right) [4]

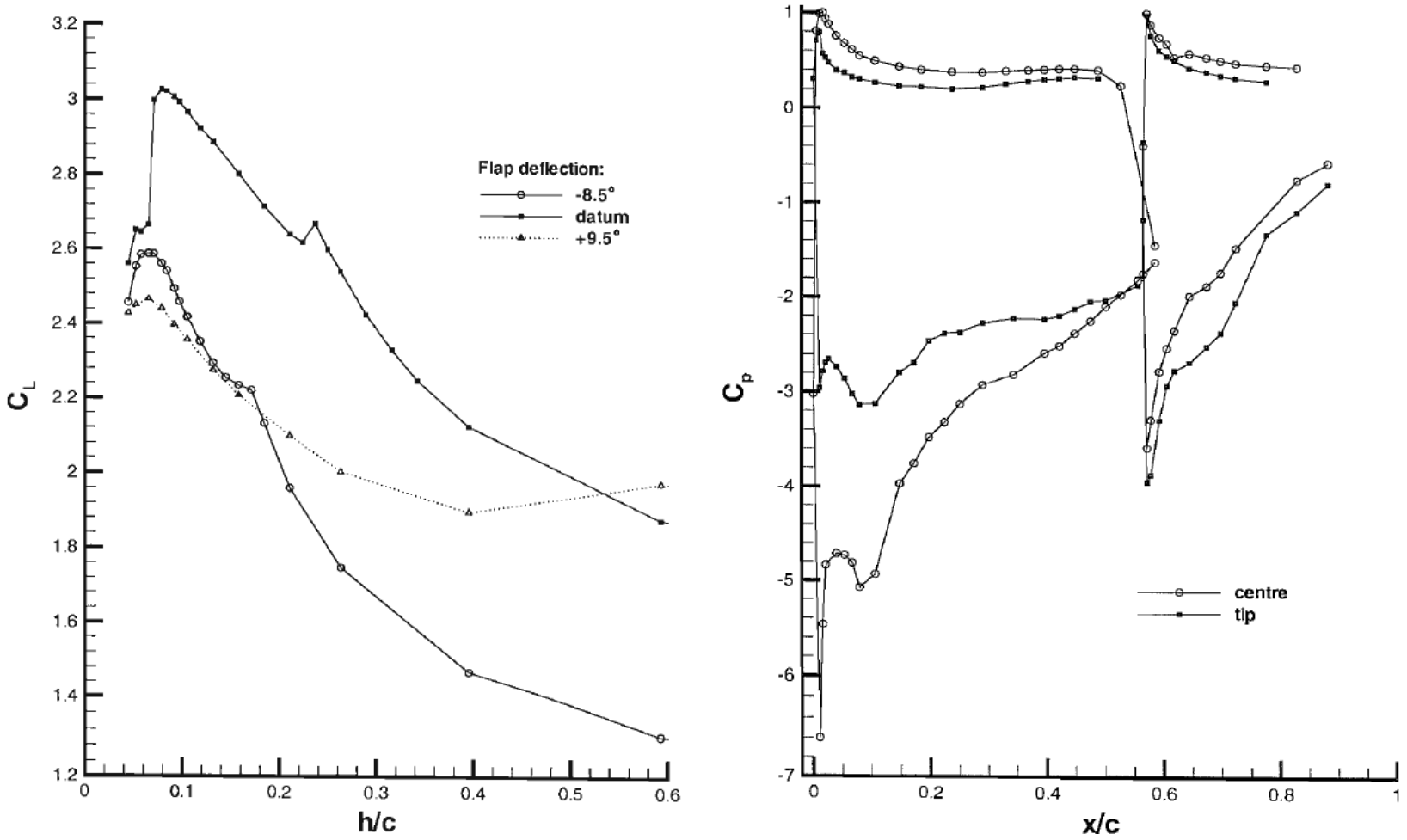

Figure 1-5. Double element wing in ground effect: Change in downforce with ground height for different flap AoA (left) and Chordwise surface pressures at centre and near to wing tip for high flap angle at h/c = 0.263 (right) [4]

1.2.3 Aeroelasticity Fundamentals

Aeroelasticity studies the interaction between inertial, elastic and aerodynamic forces [5]. Those interactions can be observed in Figure 1-6 and are classified as follows:

- Static Aeroelasticity: Elastic and aerodynamic forces.
- Structural Dynamics: Elastic and inertial forces.
- Flight Dynamics: Aerodynamic and inertial forces.
- Dynamic Aeroelasticity: Elastic, aerodynamic and inertial forces.

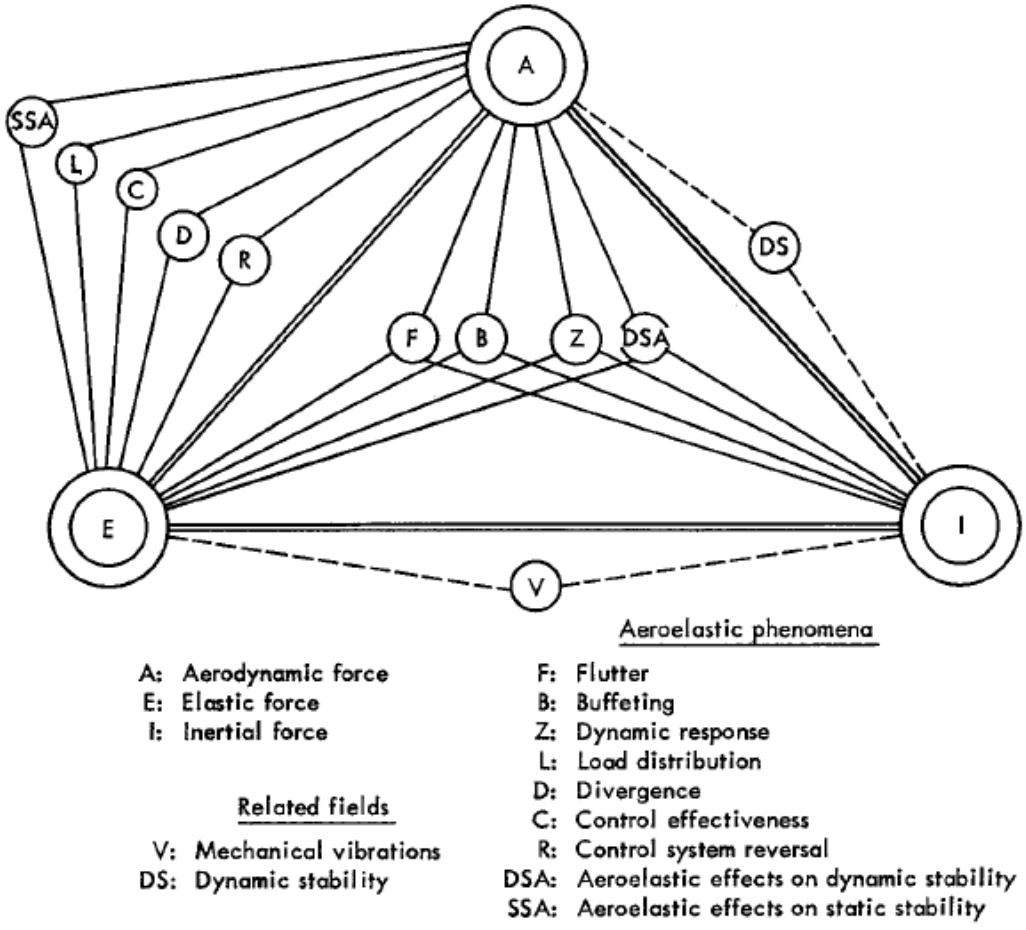

Figure 1-6 The aeroelastic triangle of forces [5]

In this project, inertial forces are not going to be considered as it is later explained in chapter 1.2.4. Therefore, this project has been focused on static aeroelasticity where in this case, divergence phenomena and material plasticity are the main concern.

1.2.4 Fluid Structure Interaction Coupling Method

Fluid Structure Interaction (FSI) solvers couple the structural and fluid solvers to solve aeroelastic problems, as it is the case of this thesis where suction surface is deformed due to aerodynamic forces and aerodynamic forces change because of surface deformation. To solve this loop FSI coupling methods are needed. And there are two main coupling methods: one-way and two-way coupling.

One-way coupling calculates first the fluid solution so that the pressure field of interest can later be used by the structural solver in order to calculate the deformation caused by the fluid. This is a stable and efficient (low computational cost) coupling, however it is limited to cases where the deformation of the structure is not large enough to produce significant changes in the flow characteristics.

Two-way coupling uses the same principle as one-way but with an additional step where the produced deformation is used to update the fluid solver geometry so that the calculation process can be repeated. To stop this cycle, convergence criteria for solution stability have to be stablished. Although this method is more computationally expensive, it is more accurate in cases where large or non-linear structural deformations with significant effect in the fluid domain occur.

- Monolithic approach: Solves the fluid and structural cases in a single domain and the equations are solved simultaneously and coupled. Nevertheless, is generally only used for research as it is often too computationally expensive [6].
- Partitioned method: Separate solvers are used for the structural and fluid analysis.
    - Weakly or loosely coupled scheme: This process does not need to reach any equilibrium converge criteria, it only requires one solution of either field per time step which must be sequentially staggered. For these reasons, this coupled scheme is considered time efficient. However, if the “added-mass effect” (inertial force) is significant, the solution may become unstable. Instabilities may

occur because of elasticity coefficients, fluid and solid density being close, or time step size being too small [6].

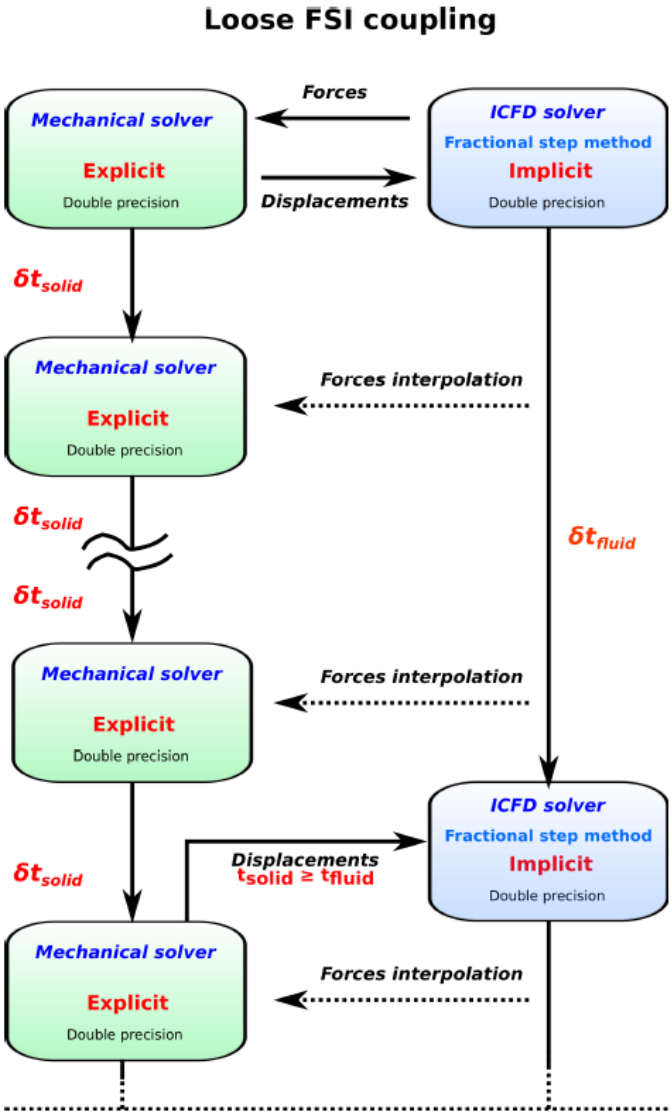

Figure 1-7. Weakly/Loosely coupled scheme [6]

- Strong coupled scheme: This process iterates between both solvers for each time step, until it reaches the convergence criteria or stablished maximum iterations. As this method is only compatible with implicit solvers [6] it cannot be used to analyse acceleration effects (inertial forces). Therefore, static aeroelasticity can only be analysed according to chapter 1.2.3.

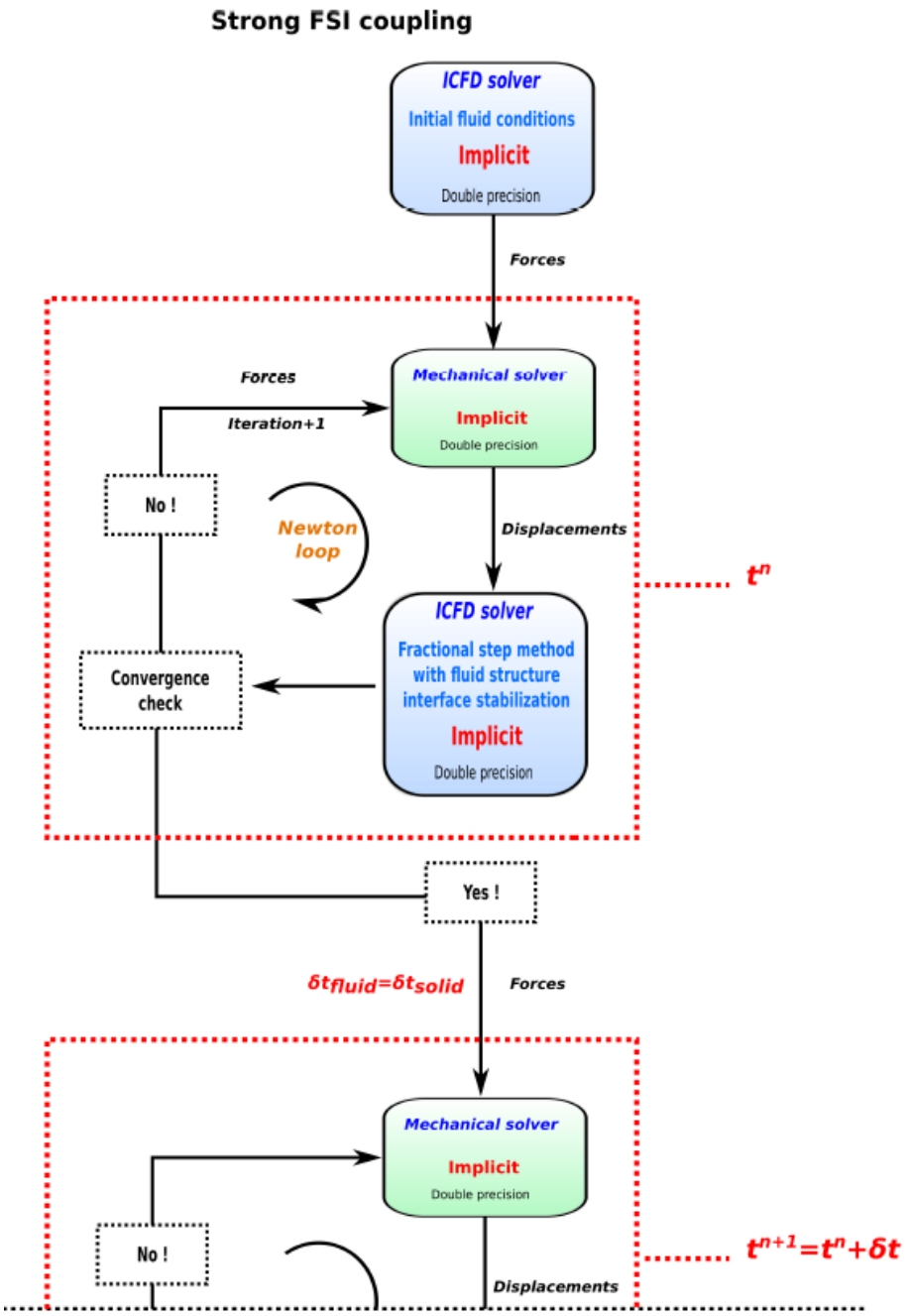

Figure 1-8. Strong coupled scheme [6]

1.2.5 Aeroelastic Tailoring

Both, in aerospace and automotive industry, the optimal aerodynamic performance specifications changes depending on the situation. Apart from pure performance, design constraints may require aeroelastic tailoring to achieve a safe design. These technical solutions are achieved through passive and active systems, as it is explained in next chapters.

1.2.5.1 Passive Systems

Passive aeroelasticity design consist of matching the pressure field and the structural design to achieve a certain aim. Several examples can be found both in aerospace and motorsport industry.

Grumman X-29 [7], see Figure 1-9, has a forward swept wing configuration that produces a twisting force while producing lift, which rotates the wing leading edge (LE) upward. This results in a higher AoA, increasing lift and therefore, twisting the wing further, leading to structural failure (divergence, chapter 1.2.3 Static Aeroelasticity). Instead of choosing conventional metallic construction to stiffen the wing, which would have increased the mass making the design unfeasible, carbon fibre was chosen. The anisotropic elastic coupling between bending and twisting of the carbon fibre was key in the decision. When the wing tips are forced to bend upward because of lift, the coupling will resist the torsion loads and twist the leading edge downwards. As a result, AoA and therefore lift will be reduced avoiding divergence.

Figure 1-9. Grumman X-29 [8]

In motorsport, restriction of active aerodynamic devices in Formula One [1] for example, force engineers to make compromises between downforce (corners: entry, apex and exit) and drag (straights), target efficiency being dependant of circuit characteristics. One of the main sources of drag is the rear wing, so by designing a rear wing mounting that has a determined bending at a target speed, AoA of rear wing is decreased reducing downforce and drag, thus increasing top speed. In Figure 1-10 regulations limitations at the beginning of 2021 F1 season are shown.

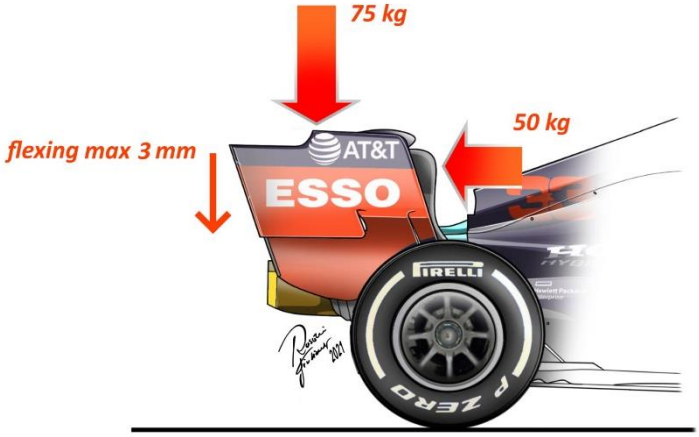

Figure 1-10. Rear wing flexing restriction according to 2021 regulations [9]

Apart from reducing drag, higher downforce can be obtained if appendices close to the ground, but limited by boundary boxes (rules, [1]), can get closer maximising ground effect as seen in chapter 1.2.2.2. This effect has been obtained by designing the wing structure so that it bends increasing ground effect (see Figure 1-11) while avoiding divergence or flutter issues.

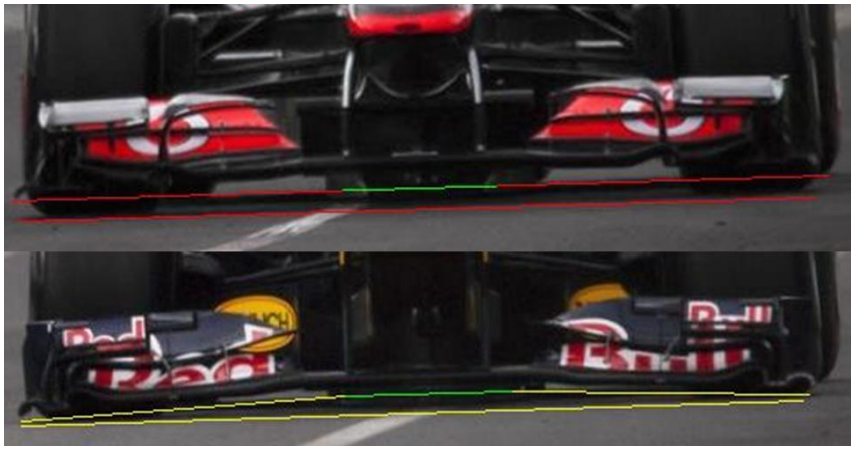

Figure 1-11. Front wing flexing RB7 (bottom) vs MP4-26 (top) [10]

1.2.5.2 Active Systems

Opposite to passive aeroelastic tailoring, pressure field is no longer a constraint but a specification for active systems design, as they will have to resist it. As these systems have more freedom and creativity, a wider range of applications are available.

In the aerospace sector active aeroelastic design is used for example in de-icing techniques as EESS (Electro-Expulsive Separation System), see Figure 1-12 [11].

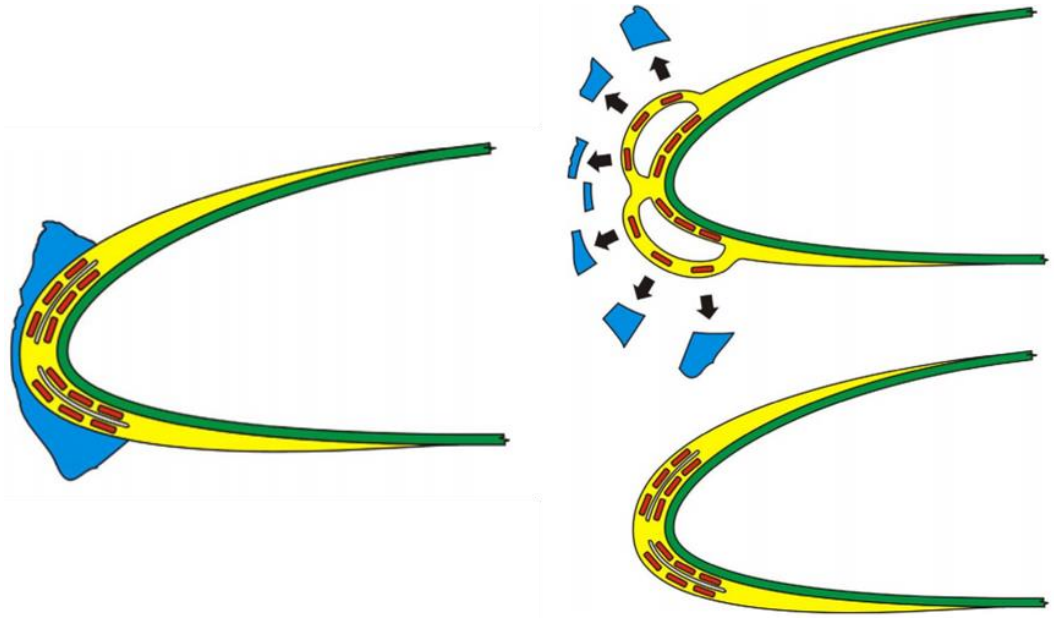

Figure 1-12. Electro-Expulsive Separation System [11]

Beyond safety, in order to reduce fuel consumption and fuel-related emissions, pressure has been placed on aviation industry. Among the different solutions, morphing wing technology can be found which consist of obtaining the best performance in any flight condition. An example is shown in Figure 1-13 where a Drop Nose Leading Edge (DNLE) and Morphing Trailing Edge (MTE) is optimised to minimise drag.

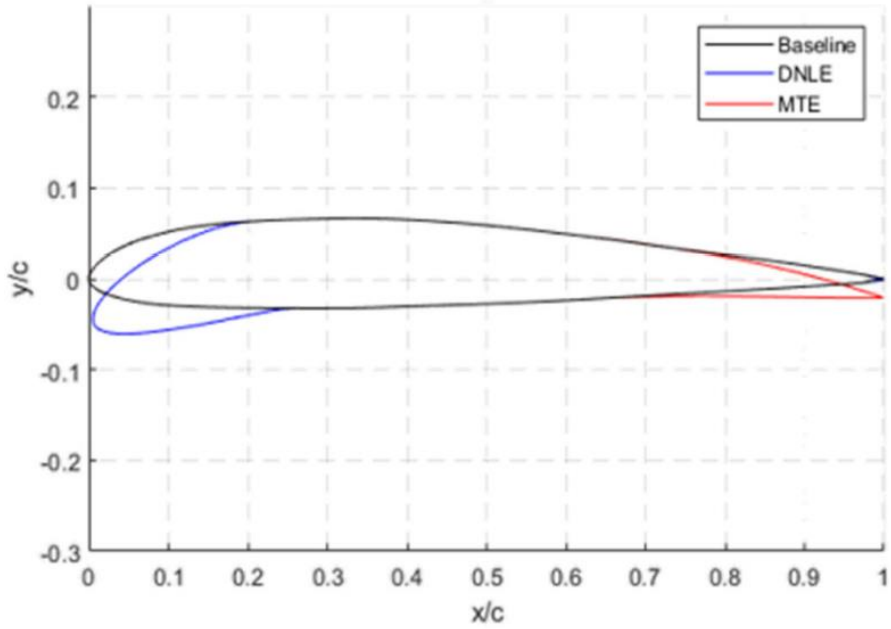

Figure 1-13. Design of DNLE and MTE airfoil compared to baseline [12]

In Formula One and many other competitions, exist an active system which is permitted by the regulations: the Drag Reduction System (DRS), see Figure 1-14. The system rotates the secondary flap moving upwards the leading edge, thus reducing the AoA and opening a gap between the main and secondary flap.

Figure 1-14. DRS closed (left) and open (right) [13]

1.3 Gap in Knowledge

As motorsport aerodynamic research tends to be confidential, there is room for further investigation based on publicly available research. Aeroelasticity based design in Motorsport has been focused on bending and twisting wings to increase downforce and efficiency. However, it has not been published research about the effects of increasing airfoil thickness through airfoil passive deformation.

1.4 Project Aim

This master thesis aims to design airfoil suction surface passive deformation to match the effects of increasing airfoil thickness on a double element wing in ground effect.

1.5 Project Objectives

- Describe the effects of suction surface deformation and relate them against thickness (t/c) increase in ground effect condition.
- Design most suitable material/lay-up to reproduce the desired deformation profile and withstand the loads.
- Study the effects of deformation profile deviations on aerodynamic key performance indicators.

2 METHODOLOGY

In this section the methodology process followed for the development of the thesis is explained. In Figure 2-1, an overview of the methodology is shown.

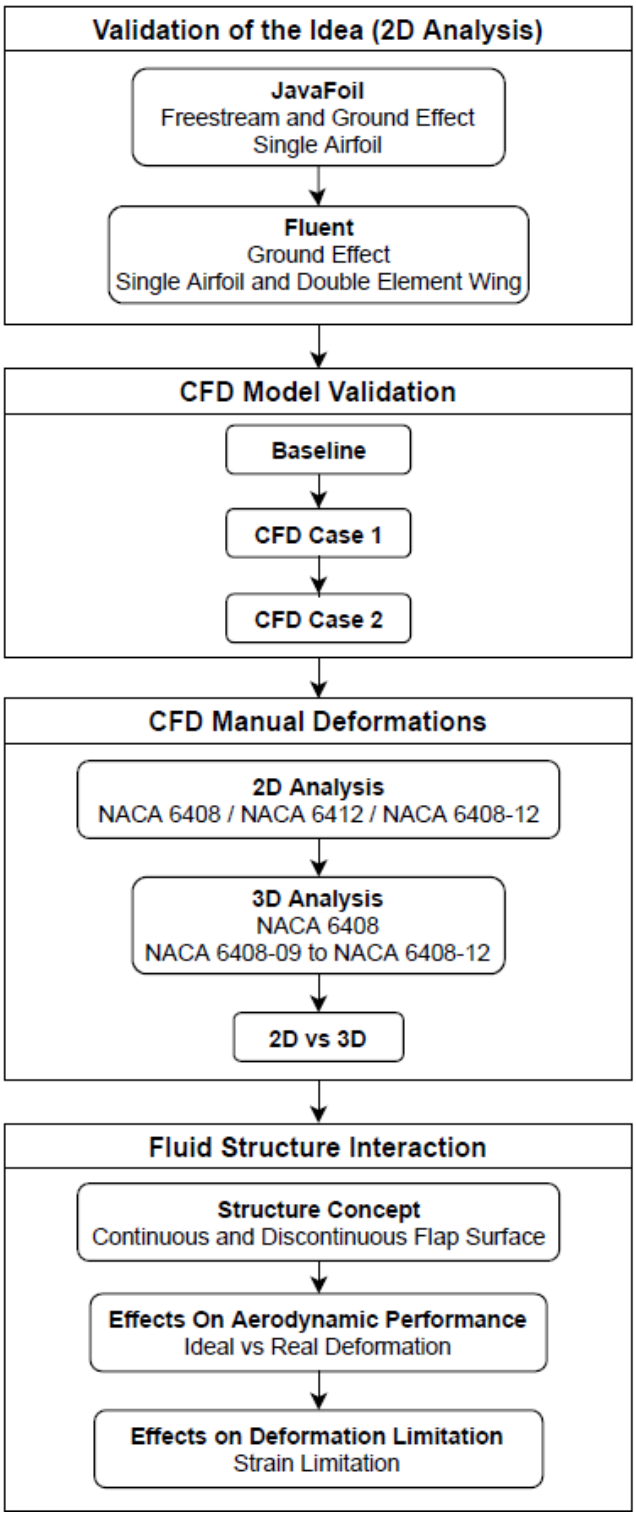

Figure 2-1. Methodology flow chart

2.1 Validation of the Idea (2D Analysis)

This first step consists of confirming with fast and simple simulations the potential of this thesis idea. The analysis was focused on observing changes in aerodynamic coefficients and pressure distribution when changing airfoil thickness and suction surface.

In this step and in 2.3, as there was no structural model, the deformation of the airfoil was manually done in CAD. The manual deformation consisted of changing the suction surface of the baseline airfoil by the same surface of that airfoil with higher thickness. For example, a NACA 6408-12, see Figure 2-2, means that the pressure surface is the same as in the baseline geometry (NACA 6408), but the suction surface is from the thickness increase (NACA 6412).

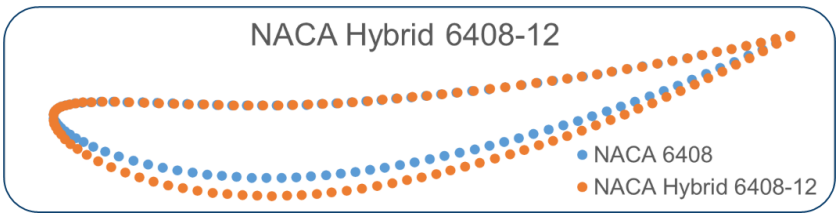

Figure 2-2. NACA 6408-12 geometry compared to NACA 6408

NACA 64 airfoils were chosen because NACA 63 airfoils (Figure 1-1) data was not available in [3], in case freestream validation was needed.

To ensure repeatability of results and make the process of changing CAD to different thicknesses fast and reliable in this step and in 2.3, NACA 4-digit airfoils were used. Points coordinates for different thicknesses could be easily obtained from JavaFoil application [14]. These coordinates were exported through an Excel macro to Catia where the fluid domain was prepared to export to ANSYS Fluent.

1. JavaFoil simulation tool [14].
    i. Increase airfoil thickness and observe Cl, L/D and pressure distribution.
    ii. Limitations: simulation do not consider flow separation. Therefore, further analysis had to be done.

2. ANSYS Fluent.
    i. Analysis closer to reality, boundary layer (wall Y+ < 5) and flow separation.
    ii. Comparison of thickness increase and suction surface deformation.

From this analysis it was concluded that a single airfoil was not appropriate for the development of the project because of the increase of APG when getting closer to the ground, resulting in flow separation.

Hence, a double element wing was simulated, and an increase in downforce and efficiency was observed when increasing thickness close to the ground. For further technical explanation please refer to chapter 3.1.

2.2 CFD Model Validation

In order to obtain reliable conclusions, it was required to understand the accuracy of the CFD model that was going to be used. As determined in the previous step, the geometry was a double element wing in ground effect conditions. Therefore, published experimental analysis of this type of geometry and conditions was sought [4]. From this PhD thesis, the CAD geometry and the pressure distribution at different ground clearances were obtained.

A ground clearance of 0.263 h/c was chosen, but there was no specific requirements other than not been an extreme ground clearance condition (close to abrupt drop in performance or flat region, see Figure 1-5) so that thickness increase could provide effectively an increase in performance.

In the pursuit of improving data correlation, different parameters from the simulation were tuned (for further explanations please refer to chapter 3.2):

a. Fluid domain dimensions.
b. Boundary conditions.
c. Mesh.
d. Turbulence model.
e. Solution methods:
    a. Pressure-velocity coupling scheme.
    b. Spatial discretisation.

2.3 CFD Manual Deformations

This step was separated in two sub-steps: 2D and 3D simulations. In both cases, the effects of increasing main airfoil thickness and suction surface passive deformation were compared.

Once NACA 6408 was defined as baseline, maximum thickness increase and hence, deformation, was limited by material maximum elastic strain value based on a continuous flap surface structure. For this reason, maximum thickness increase was set to 4% (NACA 6412), equivalent to a 1.6% strain (elastomers or low fibre fraction volume composites).

a. 2D analysis.

   The objective of this analysis was to compare main airfoil baseline geometry (NACA 6408) against NACA 6412 and the hybrid NACA 6408-12. In this analysis, the difference in aerodynamic coefficients and efficiency was observed to certify with a validated CFD model if there were performance gains and if thickness increase and surface deformation provided similar performance.

b. 3D analysis.

   Because of 3D effects, for the same geometry, less downforce and efficiency were expected. However, the objective was to find out whether this phenomenon changed the trends observed in the 2D analysis.

2.4 Fluid Structure Interaction

The first objective regarding FSI was to confirm that targeted deformation could be achieved with the combination of suction surface pressure distribution and wing structure.

Considering the different approaches explained in chapter 1.2.4, the one-way analysis was the most effective and efficient method to check if the deformation shape and tendency could match aimed deformation.

After first structure analysis, it was determined that a continuous wing surface was not the right philosophy to achieve the desired deformation, for further technical information please refer to chapter 3.4.1.1. Therefore, a discontinuous

flap surface concept was designed to achieve it. Furthermore, this structure philosophy did not have the strain limitations of the previous concept and so, higher deformations could be analysed.

Finally, a two-way strong coupling (implicit solvers) analysis of the final structure was tried in order to analyse the convergence (final solution) of the system but did not have the time to make it work. Therefore, a two-stage one-way analysis was performed. To achieve that, the deformation of the first one-way analysis was manually translated into the CAD to perform the CFD analysis of the real deformation. This step was necessary as the third objective of the thesis was to study the effects of deformation profile deviations on aerodynamic key performance indicators.

3 RESULTS AND DISCUSSION

3.1 Validation of the Idea (2D analysis)

Based on single airfoil on ground effect data [4], it is decided to simulate the NACA 6408 airfoil at h/c of 0.224, leaving room to further increase in downforce reducing ground clearance by the increase of airfoil thickness. Besides, an AoA of 10º is set maximising downforce at low ground clearances, see Figure 1-4.

3.1.1 JavaFoil

NACA 6408 airfoil has been simulated with an incidence angle of 10º, both in ground effect (h/c of 0.224) and freestream to observe differences and potential future applications to appendices far from the ground. In both cases, thickness increase effect into aerodynamic Key Performance Indicator (KPI) has been analysed. Therefore, NACA 6408 and NACA 6412 has been simulated and compared in Table 3-1 described conditions as showed in Figure 3-1 and Figure 3-2. As the reference point for translation in Y direction is the LE, ground clearance (h/c) is not exactly 0.224 (±1%) but as both cases have same error, the KPI comparison is still valid.

Table 3-1. NACA 6408 positioning for ground effect and freestream simulations

Simulation	***AoA [º]***	***h/c [-]***
Ground Effect	10	0.224
Freestream	10	N/A

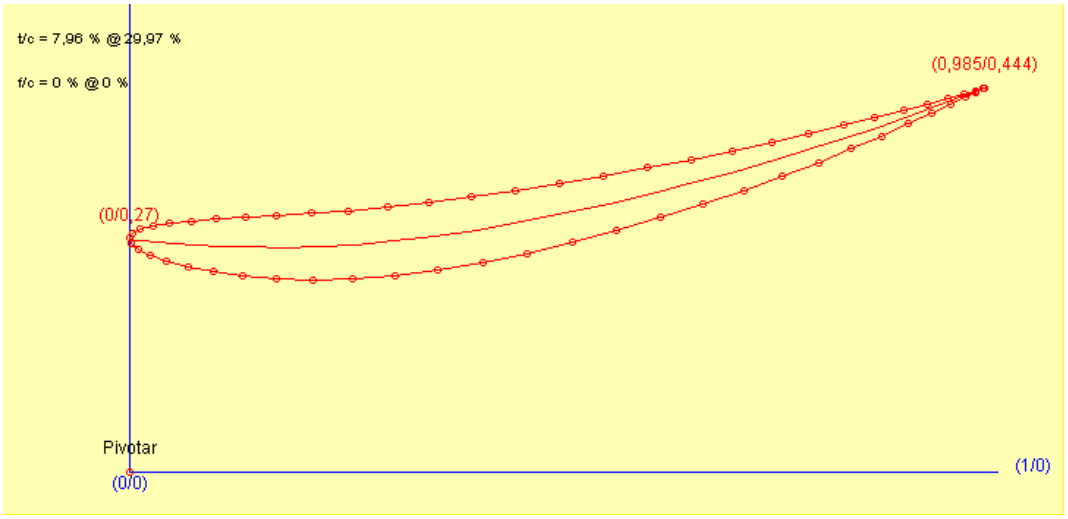

Figure 3-1. JavaFoil: NACA 6408 AoA10 in ground effect layout

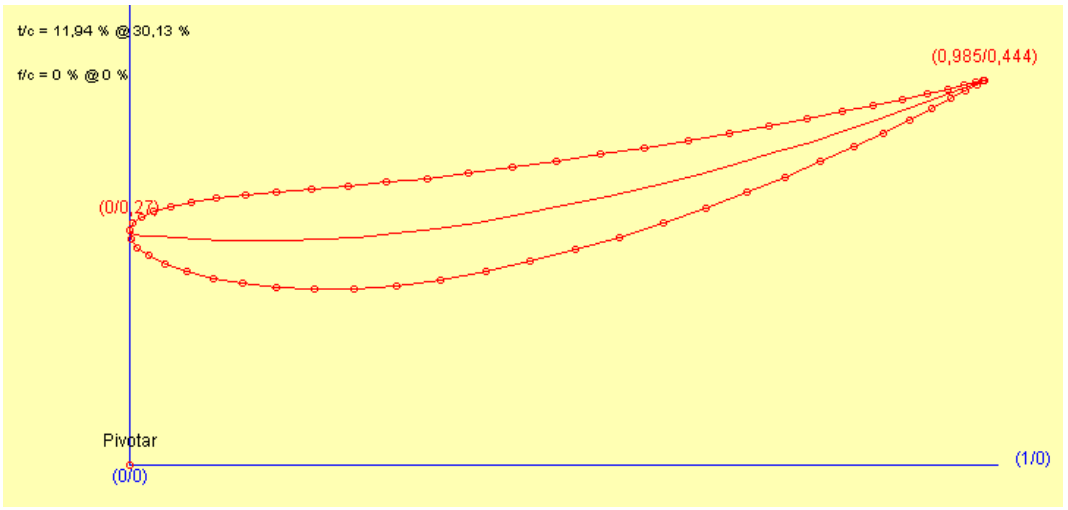

Figure 3-2. JavaFoil: NACA 6412 AoA10 in ground effect layout

Results observed in Figure 3-3 and Figure 3-4 have been summed in Table 3-2.

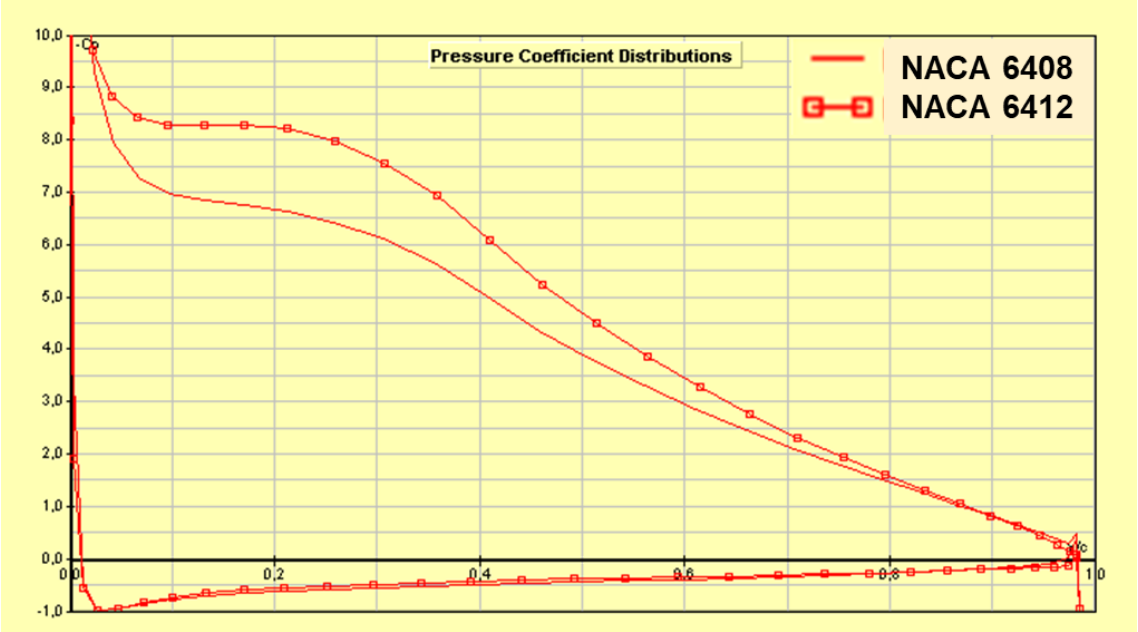

Figure 3-3. JavaFoil: NACA 6408 vs NACA 6412 AoA10 pressure coefficient distribution in ground effect

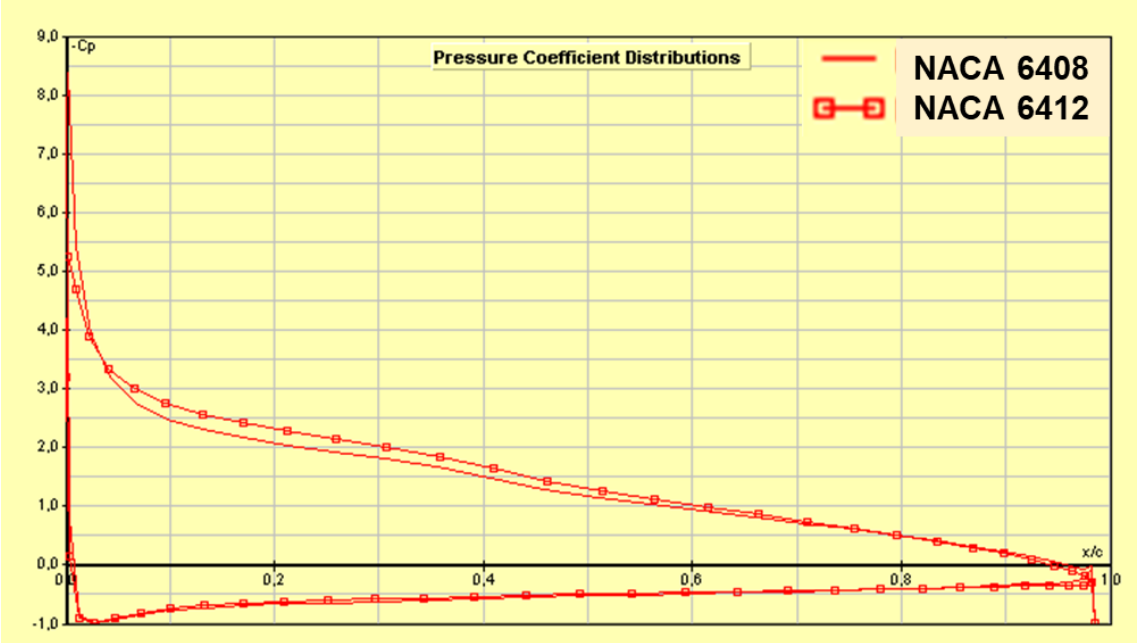

Figure 3-4. JavaFoil: NACA 6408 vs NACA 6412 AoA10 pressure coefficient distribution in freestream

Table 3-2. JavaFoil: NACA 6408 and NACA 6412 AoA10 KPI in ground effect and freestream

Ground Effect	***Cl***	***Cd***	***-L/D***
NACA 6408	-2.491	0.085	29.31
NACA 6412	-3.780 (+51.75%)	0.195	19.38 (-33.88%)
Freestream	***Cl***	***Cd***	***-L/D***
NACA 6408	-1.599	0.024	66.63
NACA 6412	-1.822 (+13.95%)	0.036	50.61 (-24.04%)

Results from Table 3-2, confirms that downforce increase and efficiency decrease when increasing airfoil thickness.

Furthermore, in ground effect, the gains and losses are bigger than in freestream, as increase in downforce is almost four times bigger in ground effect than in freestream while efficiency decrease is 1.4 times bigger.

Figure 3-3 and Figure 3-4 show that the APG in ground effect conditions is much bigger than in freestream. Besides, increasing thickness implies increasing more the APG. As explained before, JavaFoil does not consider flow separation and therefore, the results are not 100% trustworthy. For this very reason, further analysis has been carried out in the next chapter.

3.1.2 ANSYS Fluent

3.1.2.1 Single Airfoil

NACA 6408 and NACA 6412 at h/c of 0.224 has been simulated to conclude if there is flow separation and confirm the results of previous chapter.

3.1.2.1.1 Mesh

3.1.2.1.1.1 Fluid Domain

Dimensions of the fluid domain are described in Figure 3-5. Considering that flap chord length is 250 mm, 6c (six times chord length) radius from the LE has been used to define inlet and top wall and 10c from the LE to define the outlet. Besides, a refinement box has been defined with a radius of 1c upwash and 4c length downwash from the LE. This refinement box has been introduced with an angle of 5º to catch better the wake.

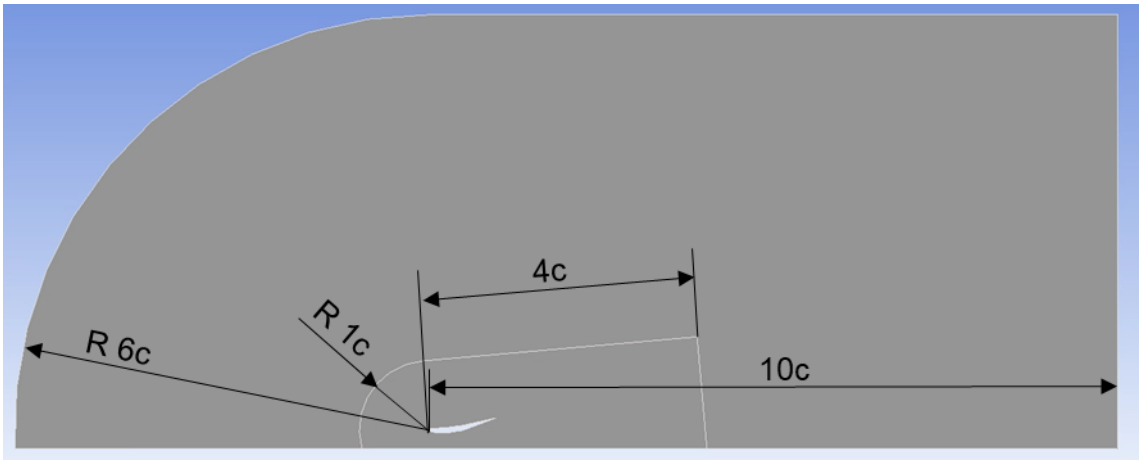

Figure 3-5. Fluent: NACA 6408 fluid domain dimensions

3.1.2.1.1.2 Mesh Setup

- Mesh size (most important parameters), see Figure 3-6:
  - Element type: Quadrilateral
  - Element order: linear
  - General element size: 20 mm
  - Curvature minimum size: 0.2 mm
  - Refinement: 5 mm
  - Growth rate: 1.2

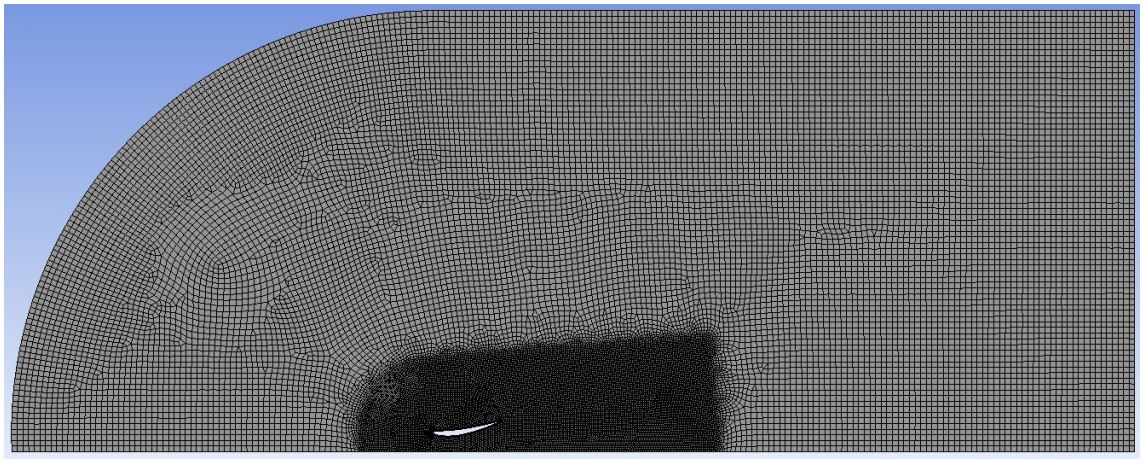

Figure 3-6. Fluent: NACA 6408 mesh overall view

- Inflation for boundary layer, see Figure 3-7:
  - Target: Wall y+ of 1 @ 30 m/s
  - Maximum thickness: 6.13 mm
  - Maximum layers: 17
  - Growth rate: 1.3

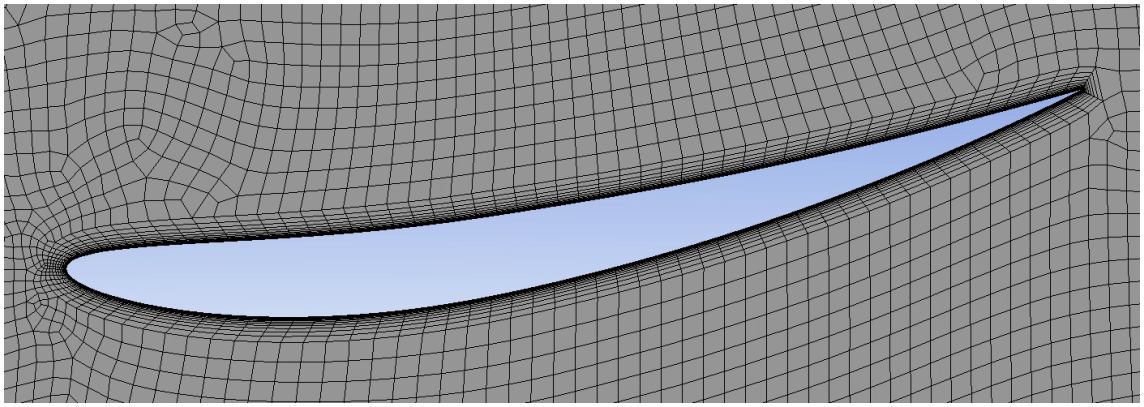

Figure 3-7. Fluent: NACA 6408 boundary layer mesh

- Nº of elements: 34,297
- Nº of nodes: 34,659

3.1.2.1.1.3 Mesh Quality

Table 3-3. Fluent: NACA 6408 mesh metrics

Mesh Metric	Average	Standard Deviation
Element Quality	0.90	0.2
Aspect Ratio	4	19.33
Skewness	0.07	0.10
Orthogonal Quality	0.98	0.05

Table 3-3 indicates the overall quality of the mesh created. All those parameters, except from the aspect ratio, were in an acceptable range. However, those values were not enough to assess the quality of the mesh. For this reason, a deeper look into the bad quality elements was done and the following was observed:

- Element Quality: The elements from the boundary layer had low quality as expected. And around 1000 additional elements (dispersed in the fluid domain) have a value lower than 0.75.
- Aspect Ratio: Apart from the elements of the boundary layer (expected) all other elements were on average 1.2.
- Skewness: 140 elements higher than 0.5 and next to the trailing edge (TE) top surface.
- Orthogonal Quality: 160 elements lower than 0.75 and in the first layers of the boundary layer in the LE and TE.

Most of the deviation of the mesh metrics were due to the boundary layer elements (unavoidable without further reducing the size of flap surface elements). Therefore, the mesh was concluded to be acceptable.

3.1.2.1.2 Solver

- Turbulence Model: SST k-ω.
- Fluid: Air
  - Density: 1.225 kg/m^3
  - Viscosity: 1.7894e-05 kg/(m·s)
- Boundary conditions (BC), see Figure 3-8:
  - Ground:
    - No slip
    - Moving wall @ 30 m/s
  - Inlet:
    - Velocity inlet @ 30 m/s
    - 5% backflow turbulent intensity
  - Outlet
    - Pressure outlet
    - 5% backflow turbulent intensity
  - Wing
    - No slip
    - Stationary wall
- Reference values:
  - Computed from inlet boundary condition (BC).
  - Area: 0.25 m^2 (same as the chord length as it is a 2D analysis).
- Methods
  - Pressure-velocity coupling
    - Scheme: coupled
  - Spatial discretisation
    - Gradient: Least squares cell based
    - Pressure: 2nd order
    - Momentum: 2nd order upwind
    - Turbulent kinetic energy: 1st order upwind
    - Specific dissipation rate: 1st order upwind
  - Steady simulation
- Convergence criteria
  - 0.001 for all residuals

Figure 3-8. Fluent: Boundary conditions

3.1.2.1.3 Results and Discussion

As stated at the beginning, NACA 6408 at 10º AoA and 0.224 h/c ground clearance was simulated. Figure 3-9 shows that flow separation happened before the 60% of the chord was reached, as suction surface wall shear stress reached the value of 0 Pa. Because of flow separation, the airfoil did not perform as predicted by JavaFoil as seen in Figure 3-3 and Figure 3-10. Therefore, that configuration was not appropriate for the development of the project.

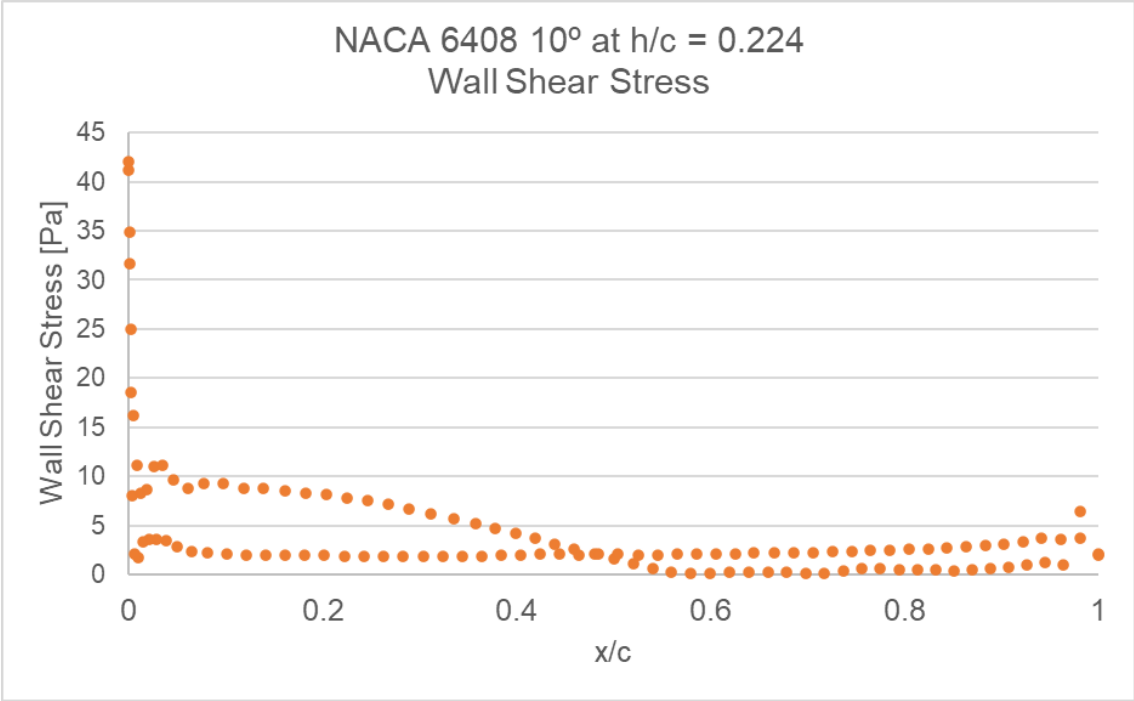

Figure 3-9. Fluent: NACA 6408 AoA 10º wall shear stress

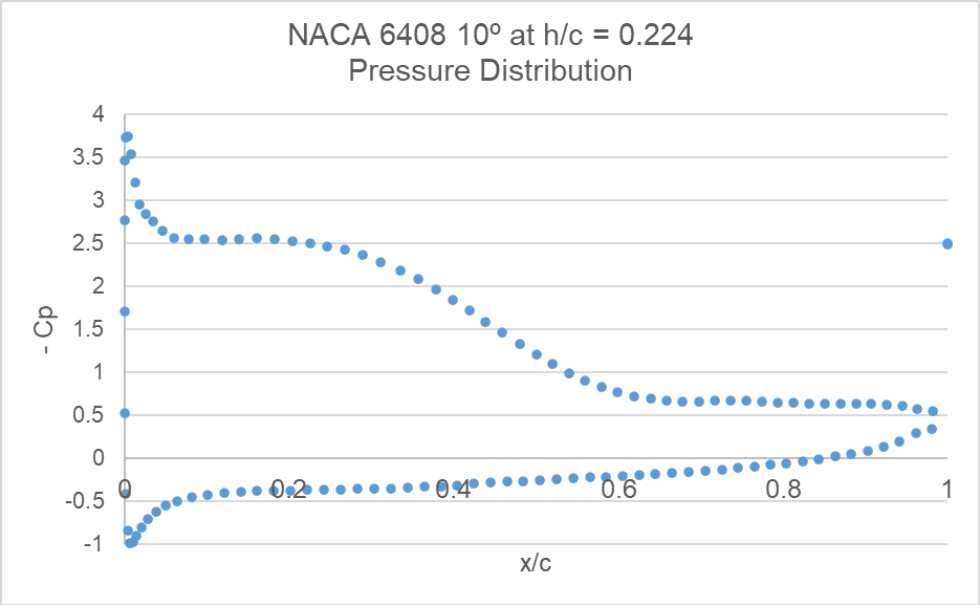

Figure 3-10. Fluent: NACA 6408 AoA 10º pressure distribution

As 10º of AoA did not work because of flow separation, 0º and 5º were also simulated.

First, 0º AoA was analysed targeting a configuration without flow separation. However, as observed in Figure 3-11, the stagnation point (Cp = 1) is found in the suction surface. This positive pressure in the suction surface would not allow achieving the targeted passive deformation and therefore this configuration was discarded.

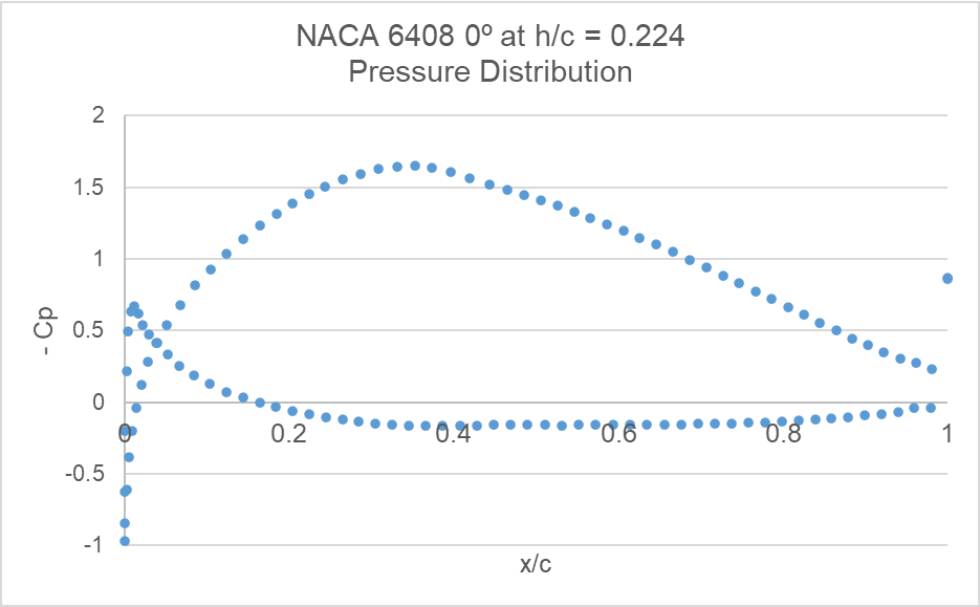

Figure 3-11. Fluent: NACA 6408 AoA 0º pressure distribution

Finally, 5º AoA was analysed as middle term between the previous simulations. Results in Figure 3-12 showed that this configuration was also suffering of flow separation, but this happened later than with 10º of AoA as expected, 80% against 60% of the chord. To confirm that these configurations were not right for the development of the project, 5º configuration was simulated once again increasing maximum thickness from 8% to 12% t/c. However, Figure 3-12 showed that flow separation happened sooner and Figure 3-13 confirmed that as a result, performance dropped.

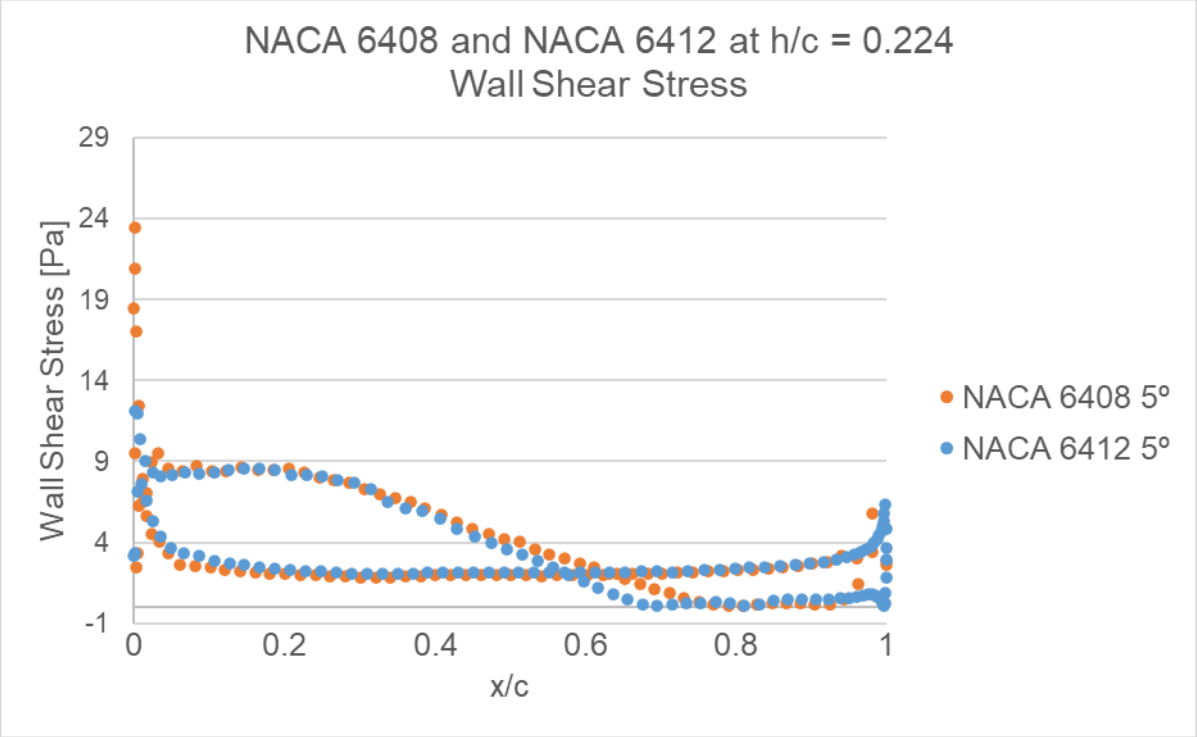

Figure 3-12. Fluent: NACA 6408 and NACA 6412 AoA 5º wall shear stress

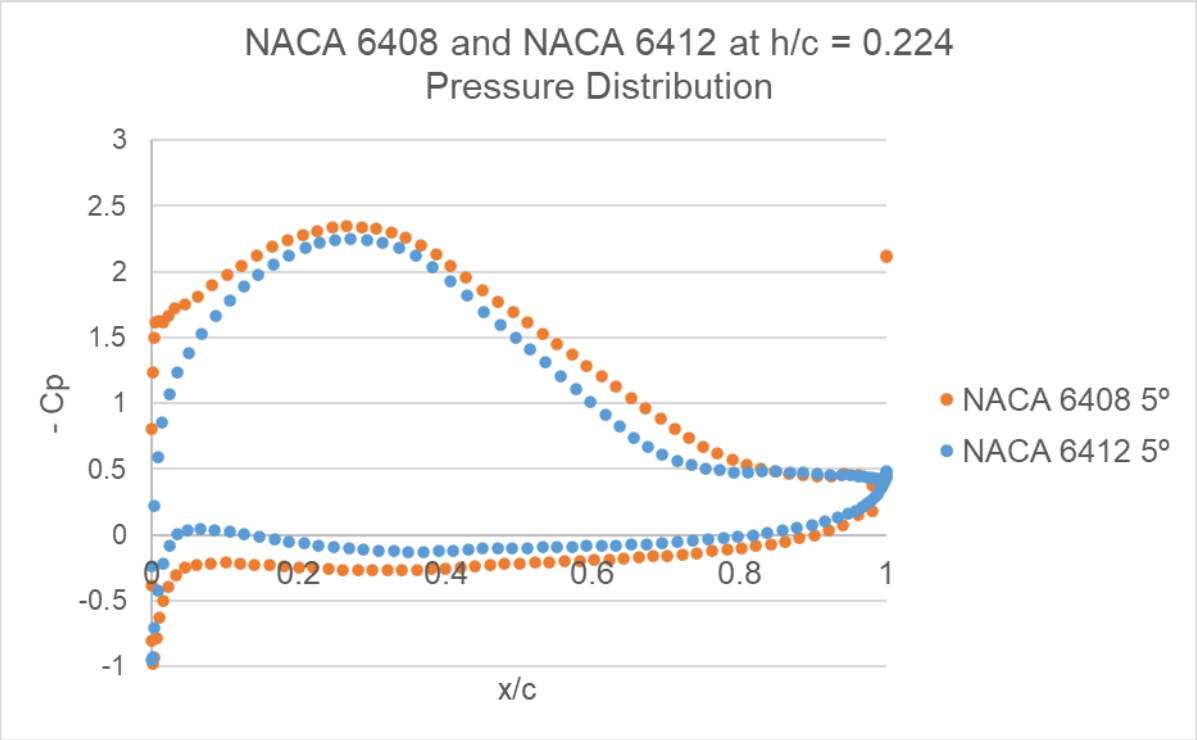

Figure 3-13. Fluent: NACA 6408 and NACA 6412 AoA 5º pressure distribution

3.1.2.1.4 Conclusions

Based on these results, it was deemed that a single airfoil was too sensitive to the increase of APG due to ground effect and therefore not suitable for the development of this project. Consequently, a new double element wing configuration was created and analysed in search of an appropriate wing configuration for this project.

3.1.2.2 Double Airfoil

Following the discussion from previous chapter, a double element wing was created. The double element wing layout can be observed in Figure 3-14 and the values of presented parameters are shown in Table 3-4. It is important to stress that this configuration was not optimised before this analysis and was not going to be optimised if no flow separation in the main flap was observed when transitioning the main flap from NACA 6408 to NACA 6412.

For the non-dimensionality of results, a total chord length of 418 mm was used. The ground clearance (h) was 200 mm because h/c was set to 0.478. This was decided to reduce the APG compared to the single airfoil, in combination with the use of second element.

NACA 6408, NACA 6412 and NACA 6408-12 as main flap were analysed.

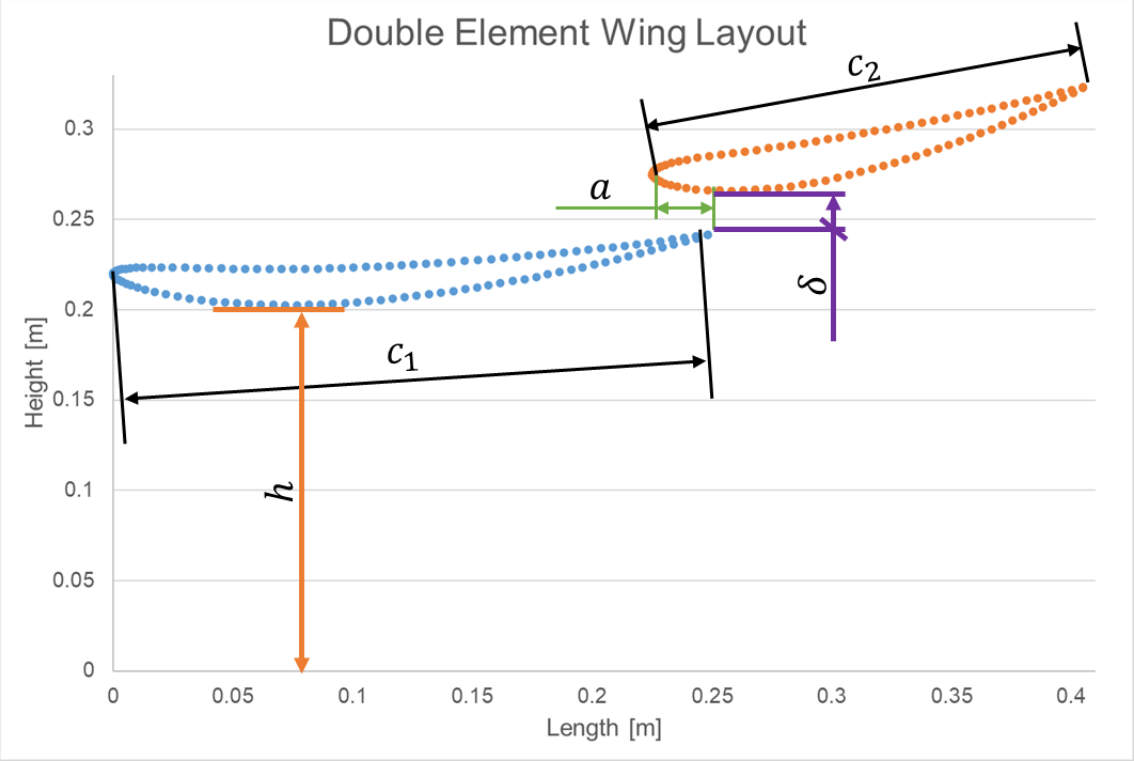

Figure 3-14. Double element wing layout

Table 3-4. Double element wing layout parameters

Parameters	Main Flap (1)	Flap (2)	Other
Airfoil	NACA 6408	NACA 6412	-
c [mm]	250	$0.75*c_1 = 187.5$	-
AoA [º]	5	15	-
a [mm]	-	-	$0.1*c_1 = 25$
δ [mm]	-	-	$0.1*c_1 = 25$
h [mm]	-	-	200

3.1.2.2.1 Mesh

Fluid Domain and mesh were built following the same procedure as in the single airfoil example.

3.1.2.2.1.1 Mesh Quality

Table 3-5. Fluent: Double element wing mesh metrics

Mesh Metric	Average	Standard Deviation
Element Quality	0.90	0.21
Aspect Ratio	2.85	9.86
Skewness	0.07	0.11
Orthogonal Quality	0.98	0.05

Table 3-3 indicates the overall quality of the mesh created. All those parameters, except from the aspect ratio, were in an acceptable range. However, those values were not enough to assess the quality of the mesh. For this reason, a deeper look into the bad quality elements was done and the following was observed:

- Element Quality: The elements from the boundary layer had low quality as expected. And around 1000 additional elements (dispersed in the fluid domain) have a value in between 0.75 and 0.55.
- Aspect Ratio: Apart from the elements of the boundary layer (expected) all other elements were on average 1.2.
- Skewness: 25 elements higher than 0.5 dispersed in the fluid domain.
- Orthogonal Quality: 250 elements lower than 0.75 in the TE and LE boundary layer.

Most of the deviation of the mesh metrics were due to the boundary layer elements (unavoidable without further reducing the size of flap surface elements). Therefore, the mesh was concluded to be acceptable.

3.1.2.2.2 Solver

Same solver configuration as for the single airfoil example was used. Being the reference area for the non-dimensionality of results (total chord length of 418 mm for the 2D analysis) the only difference.

3.1.2.2.3 Results and Discussion

Convergence of results is not excellent, but it is good as residuals are almost constant or smoothly decreasing while continuity (biggest value of all residuals) is 1e-3 as observed in Figure 3-15. Furthermore, in Figure 3-16 lift coefficient convergence is shown which is almost constant for the last 30 iterations.

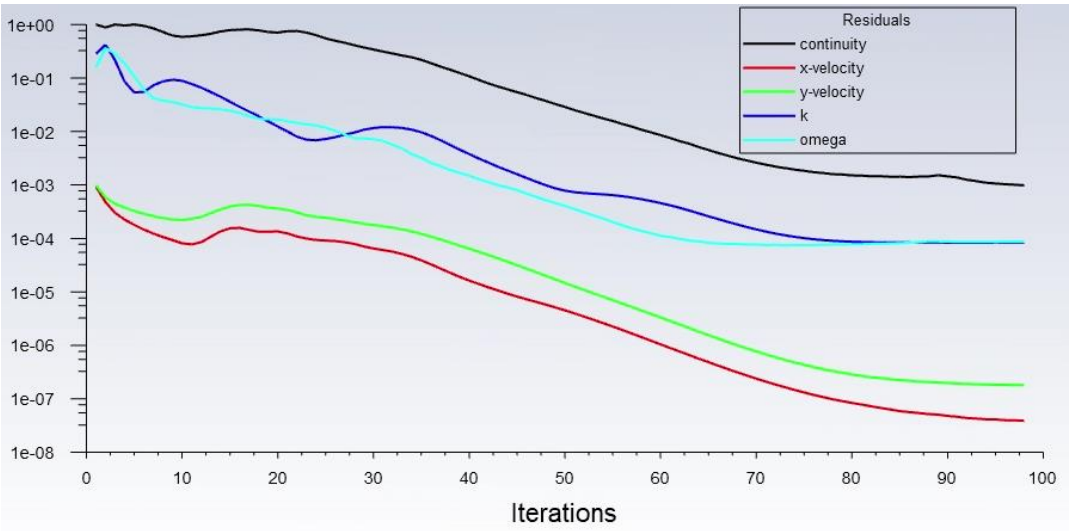

Figure 3-15. Fluent: Double element wing NACA 6412 residuals

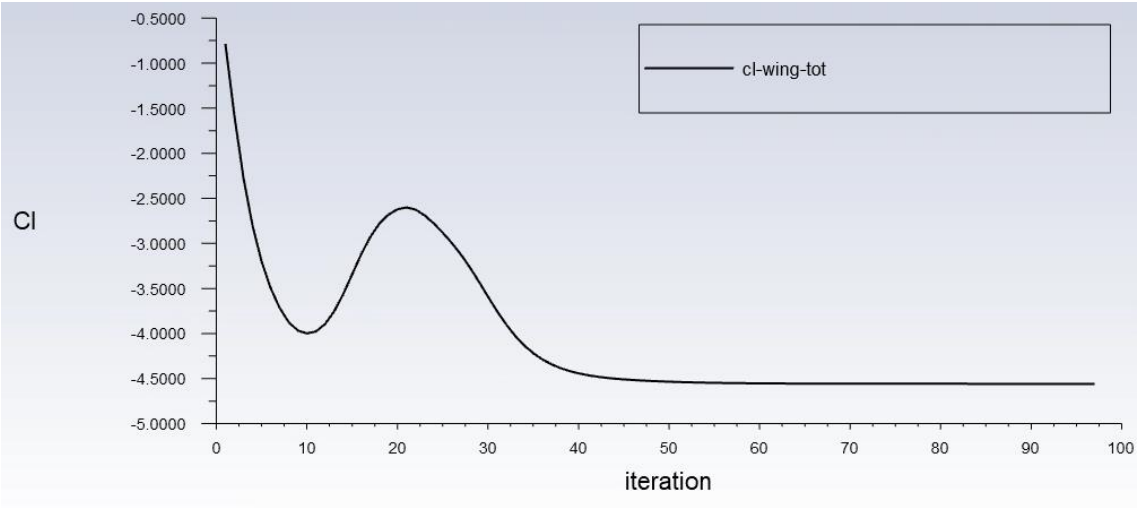

Figure 3-16. Fluent: Double element wing NACA 6412 Cl convergence

As mentioned before, three main flap configurations were simulated to analyse the effects of increasing airfoil thickness and compare those to the deformation of suction surface. In Figure 3-17, KPI values for these 3 configurations are presented. From this analysis, when increasing airfoil thickness, an increase in wing created downforce was observed, which was a consequence of the main flap downforce increase. This increase in downforce combined with a small decrease in drag resulted into an increase in efficiency. Therefore, in this 2D analysis, an increase in thickness was beneficial for the KPI of the wing.

Furthermore, in the graph is observed that the suction surface deformation (NACA 6408-12) provided an increase in performance, close to the increase in thickness (NACA 6412). Producing 1.1% more downforce but at the same time 2.1% more drag, resulting into a 1% smaller efficiency compared to the increase in thickness.

This similarity in performance between the increase in thickness (NACA 6412) and the suction surface deformation (NACA 6408-12) can be further appreciated in Figure 3-18 pressure distribution, where the difference is minimal.

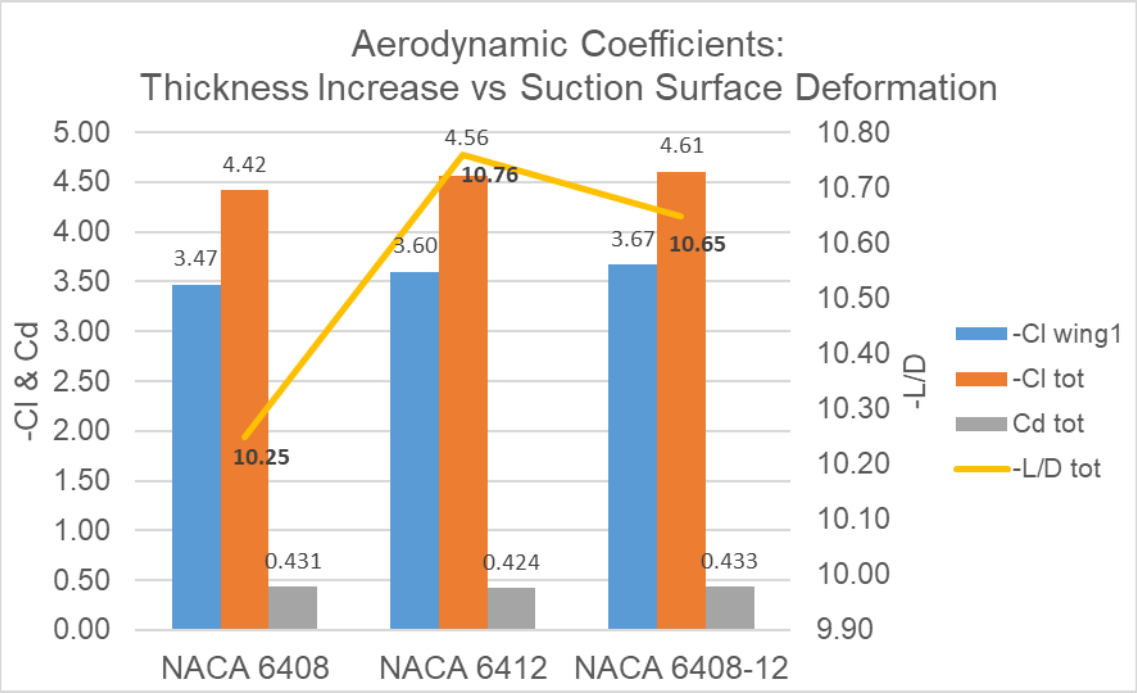

Figure 3-17. Fluent: Double element wing aerodynamic coefficients change with thickness increase and suction surface deformation

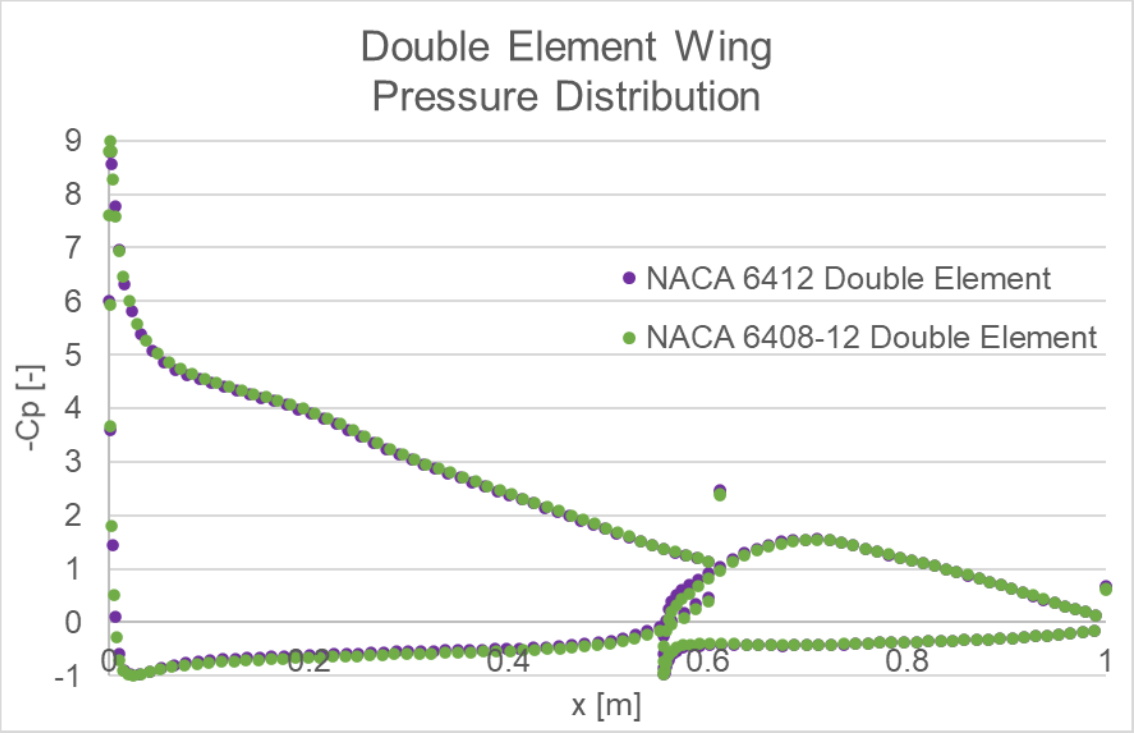

Figure 3-18. Fluent: Double element wing pressure distribution comparison, thickness increase against suction surface deformation

3.1.2.2.4 Conclusions

As summary, the double element wing configuration was proved to increase performance increasing main flap airfoil thickness and with suction surface deformation (under non reliable/validated CFD model). Hence, based on a double element wing in ground effect configuration, a CFD model validation was required to obtain reliable conclusions from this point on.

3.2 CFD Model Validation

3.2.1 CAD Model

The CAD model used for the validation was obtained from [4], which wing coordinates have been indicated in Appendix A. Taking advantage of symmetry condition under straight line wind, the wing has a span of 550 mm with an endplate of 400x170x4 mm. The chord of the main flap is 223.4 mm while flap chord is 165.7 mm, resulting in a total chord length of 378.9 mm. For simplicity, a chord of 380 mm has been considered for the non-dimensionalisation of the results [4]. As previously mentioned, a ground clearance of h/c 0.263 was chosen.

3.2.2 Baseline CFD Case

As the developed CFD model in this stage was later going to be used in more CFD and FSI simulations, the lowest computational cost but still accurate CFD model was desired. For this reason, in this baseline configuration, a low computational cost approach was followed.

3.2.2.1 Mesh

3.2.2.1.1 Fluid Domain

Dimensions of the fluid domain showed in Figure 3-19 are described in Table 3-6. For table reference, as stated before, c stands for wing total chord length that in this case is defined as 380 mm. The purpose of this layout was to calculate the smallest changes in the domain close to flaps and early stages of the wake.

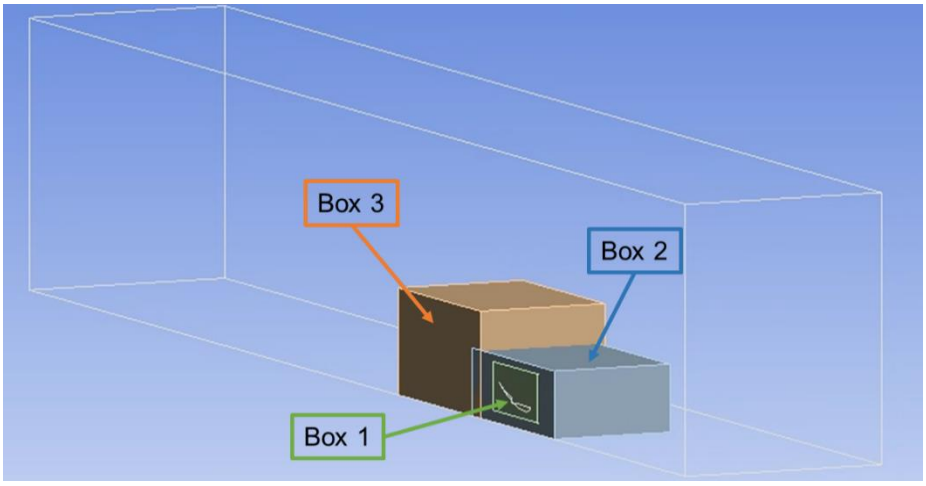

Figure 3-19. CFD Model Validation: Baseline fluid domain overview

Table 3-6. CFD Model Validation: Baseline fluid domain dimensions

	Length [mm]	Width [mm]	Height [mm]
General	5c Upstream 15c downstream	2b	3c (From flap TE)
Box 1	550	600	250
Box 2	1000	650	350
Box 3	1000	700	550

3.2.2.1.2 Mesh Setup

- Mesh size (most important parameters), see Figure 3-6:
  - Element type: Tetrahedral
  - Element order: linear
  - General element size: 150 mm
  - Curvature minimum size: 1 mm
  - Flaps:
    - LE and TE: 1 mm
    - Other: 5 mm
  - Refinement:
    - Box 1: 5 mm
    - Box 2: 10 mm
    - Box 3: 50 mm
  - Growth rate: 1.2

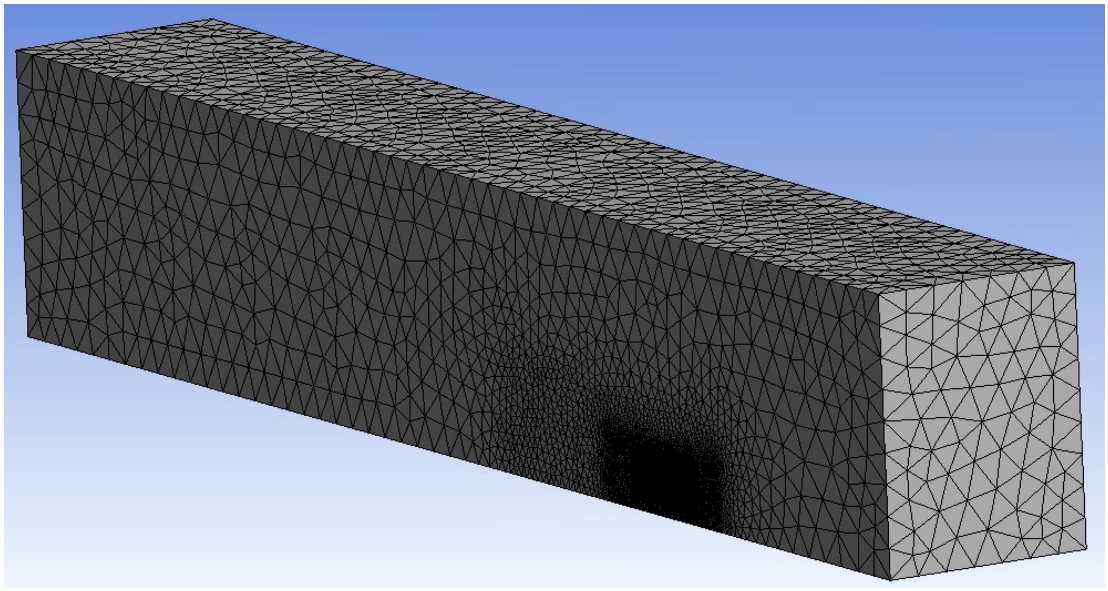

Figure 3-20. CFD Model Validation: Baseline mesh overall view

- Inflation for boundary layer, see Figure 3-7:
  - Target: Wall y+ of 1 @ 30 m/s
  - Main Flap
    - Maximum thickness: 5.57 mm
    - Maximum layers: 17
    - Growth rate: 1.3
  - Flap
    - Maximum thickness: 4.31 mm
    - Maximum layers: 17
    - Growth rate: 1.3

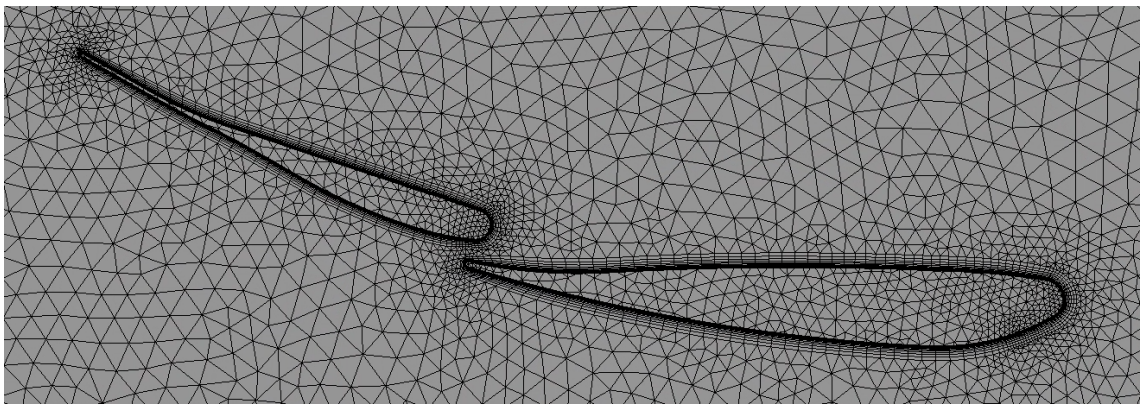

Figure 3-21. CFD Model Validation: Baseline boundary layer mesh

- Nº of elements: 5.3e6
- Nº of nodes: 1.7e6

3.2.2.1.3 Mesh Quality

Table 3-7. CFD Model Validation: Baseline mesh metrics

Mesh Metric	Average	Standard Deviation
Element Quality	0.90	0.2
Aspect Ratio	19.04	44.75
Skewness	0.25	0.15
Orthogonal Quality	0.74	0.16

Table 3-3 indicates the overall quality of the mesh created. All those parameters, except from the aspect ratio, were in an acceptable range. However, those values were not enough to assess the quality of the mesh. For this reason, a deeper look into the bad quality elements was done and the following was observed:

- Element Quality: The elements from the boundary layer had low quality as expected. And around 40000 additional elements in the refinement boxes have a value lower than 0.5.
- Aspect Ratio: Apart from the elements of the boundary layer (expected because of the difference between layers thickness and flap surface mesh) 53% of elements are average 2.1 and 1.4e5 are average 4.
- Skewness: 2e5 elements higher than 0.5 mostly in the refinement boxes.
- Orthogonal Quality: 3e5 elements lower than 0.5 mostly in the refinement boxes.

Effects of mesh quality will be analysed in next CFD cases when changing mesh parameters.

3.2.2.2 Solver

- Turbulence Model: SST k-ω.
- Fluid: Air
  - Density: 1.225 kg/m^3
  - Viscosity: 1.7894e-05 kg/(m·s)
- Boundary conditions, see Figure 3-22:
  - Ground:
    - No slip, Moving wall @ 30 m/s
  - Inlet:
    - Velocity inlet @ 30 m/s
    - 5% backflow turbulent intensity
  - Outlet:
    - Pressure outlet
    - 5% backflow turbulent intensity
  - Wing:
    - Stationary wall, no slip
  - Wall:
    - Slip
  - Symmetry
- Reference values:
  - Computed from inlet boundary condition (BC).
  - Area: 1 m^2 (for simplicity of mathematical operations).
- Methods
  - Pressure-velocity coupling
    - Scheme: coupled
  - Spatial discretisation
    - Gradient: Least squares cell based
    - Pressure: 2^{nd} order
    - Momentum: 2^{nd} order upwind
    - Turbulent kinetic energy: 1^{st} order upwind
    - Specific dissipation rate: 1^{st} order upwind
  - Steady simulation
- Convergence criteria: 1e-3 for all residuals

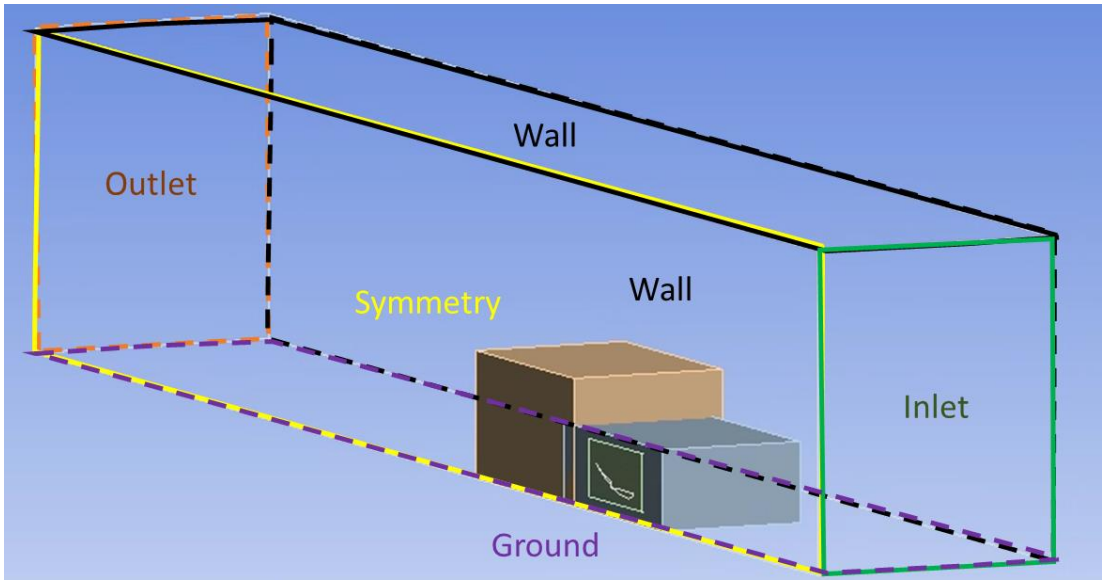

Figure 3-22. CFD Model Validation: Baseline boundary conditions

3.2.2.3 Results and Discussion

As observed in Figure 3-23, residuals did not reach acceptable values, hence, this simulation did not converge. Therefore, even if results had been accurate, they would have not been reliable. Nevertheless, as seen in Figure 3-24, obtained pressure distribution did not match the experimental data from [4] with an error in the suction surface (surface of interest for this project) in between 4.5% (peak suction) and 23.4% (concave minimum, x/c of 0.05).

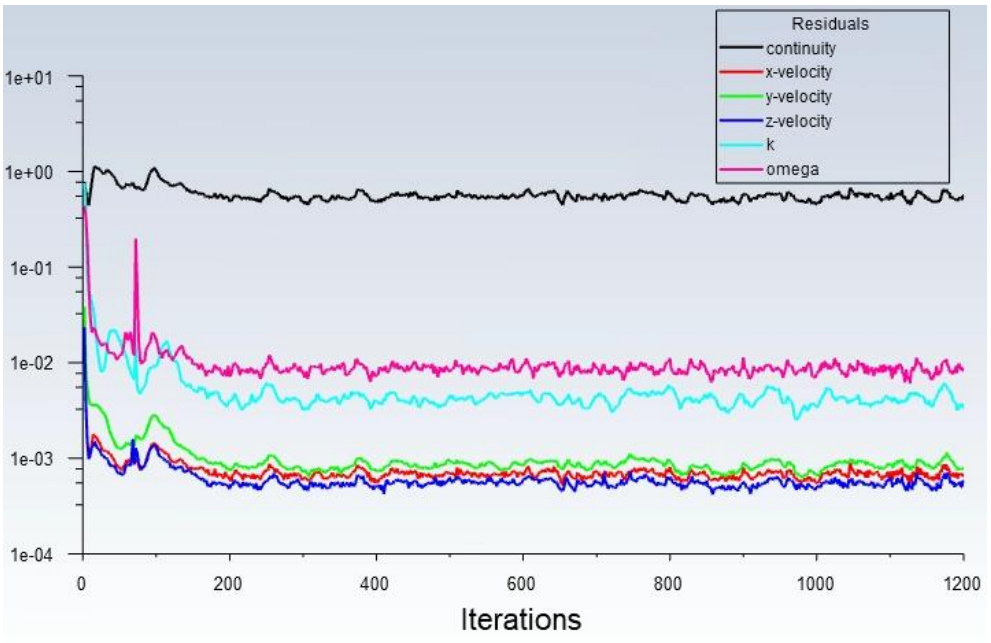

Figure 3-23. CFD Model Validation: Baseline residuals

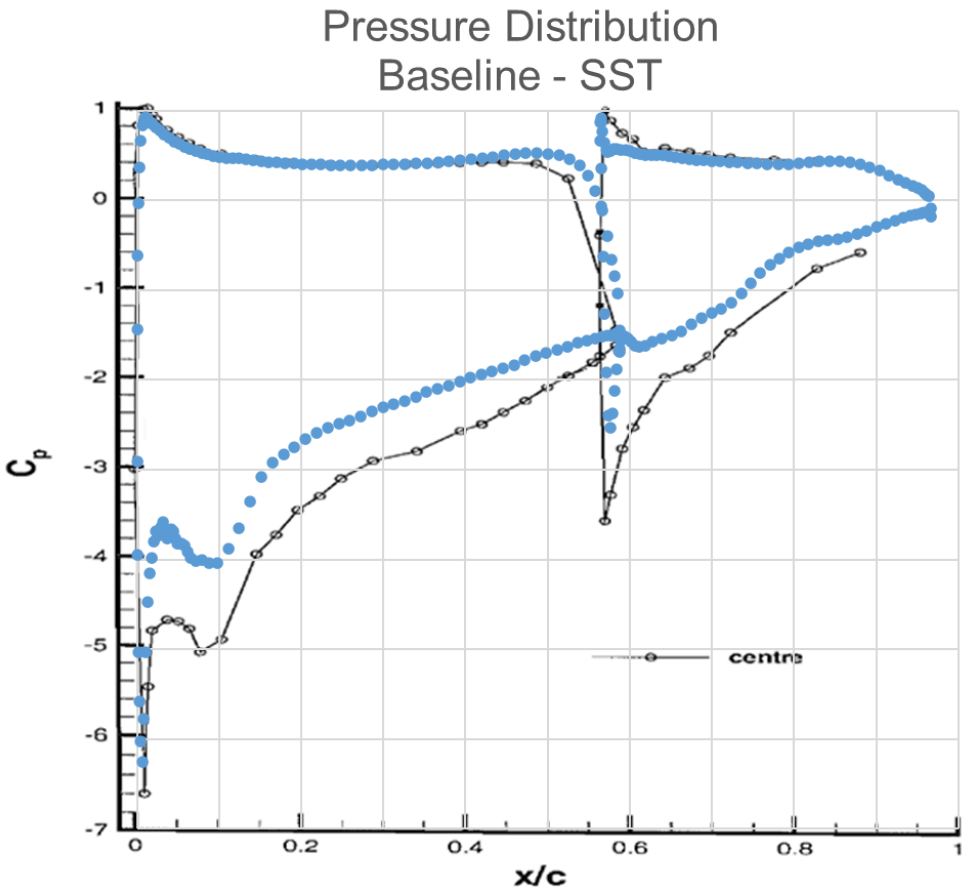

Figure 3-24. CFD Model Validation: Baseline pressure distribution (blue) compared to experimental data from the literature (black) [4]

To understand if the lack of convergence and accuracy was an issue related to the fluid domain and mesh definition or turbulence model, different RANS solver configurations were tried:

- K-epsilon: standard, realizable and RNG.
- K-omega
- SST 4 equations

Results are not presented as they did not improve neither results nor convergence.

3.2.2.4 Conclusions

Based on highlighted results and discussion, it was concluded that the fluid domain and mesh were not enough to solve the solution accurately and with good convergence. Besides, k-ω SST turbulence model obtained best convergence and accuracy for the given mesh setup.

3.2.3 CFD Case 1

3.2.3.1 Intent

Capture with more precision wake's off-body flow structures and reduce the influence of boundary conditions on the model to increase the accuracy and convergence of the simulation.

3.2.3.2 Changes made

Necessary changes were discussed with Dr. Zeeshan Rana (Cranfield University CFD course director) and it was decided to modify as follows:

- Fluid domain and mesh: 20 times the chord length in all directions (wing as reference point) and wake refinement through all the downstream. Because of limited computer resources (Intel ® Core™ i7-7700 CPU @ 3.6 GHz, 16 GB RAM), the refinement was limited to a total number of cells of 17 million. See Figure 3-25, Figure 3-26 and Table 3-8 for fluid domain update details and Table 3-9 for mesh parameters update details.
- Turbulence model: add curvature correction and change to GEKO (Generalised K-omega) turbulence model, which according to [15], by using default values same response as k-ω SST is obtained. The reason to change, was to have more freedom, if needed, to tune flow separation by using CSEP parameter.
- Solution methods (spatial discretisation): Changes were made to improve convergence at the expense of accuracy.
    - Gradient to "Green-gauss node based".
    - Pressure to "PRESTO!".
    - Momentum to "First order upwind".

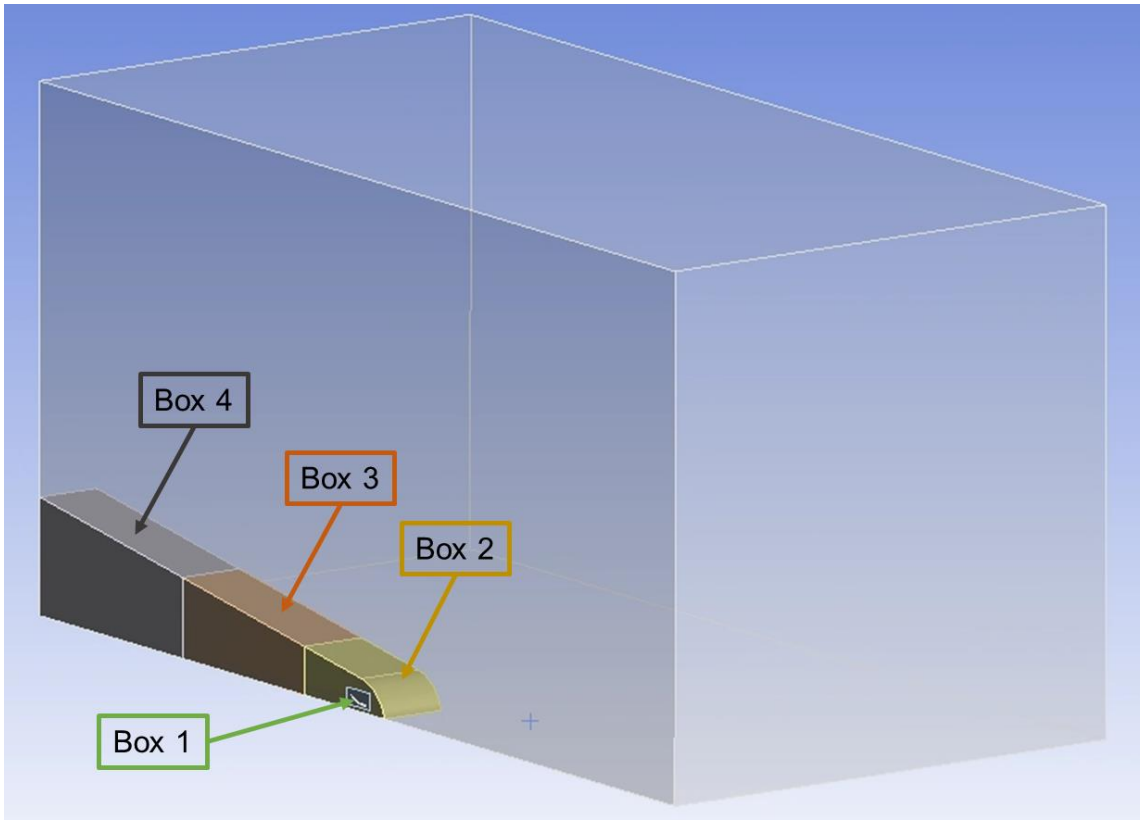

Figure 3-25. CFD Model Validation: CFD Case 1 fluid domain overview

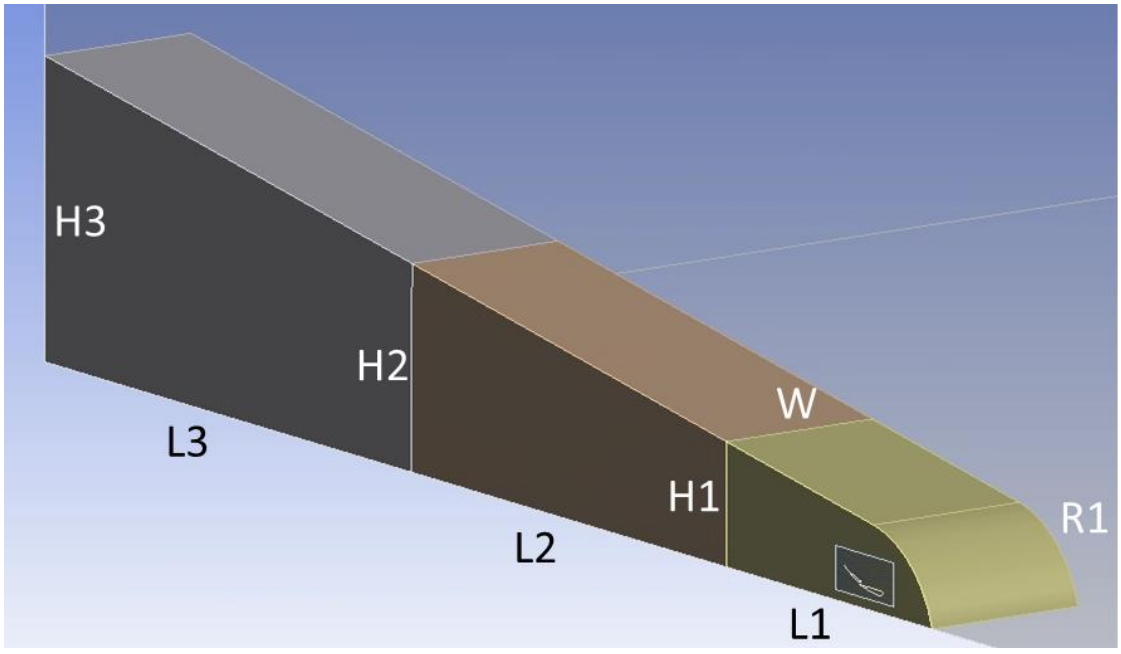

Figure 3-26. CFD Model Validation: CFD Case 1 fluid domain boxes parameters

Table 3-8. CFD Model Validation: CFD Case 1 fluid domain boxes parameters

Subscript	L [mm]	H [mm]	W [mm]	R [mm]
1	1965	714	1000	500
2	3000	1190	-	-
3	3500	1744	-	-

Table 3-9. CFD Model Validation: CFD Case 1 mesh boxes parameters

CFD Case 1	Element Size [mm]
Box 1	10
Box 2	15
Box 3	20
Box 4	25

3.2.3.3 Results

Fluid domain and mesh update affected mesh metrics. Change in mesh metrics can be observed in Table 3-10 and it can be appreciated that all mesh metrics average value and standard deviation have improved, except for element quality. This could be due to the bigger elements in box 1, which would adapt worse to the wing (trade-off because of computational limitation). For better visualisation of changes effect in wake refinement see Figure 3-27.

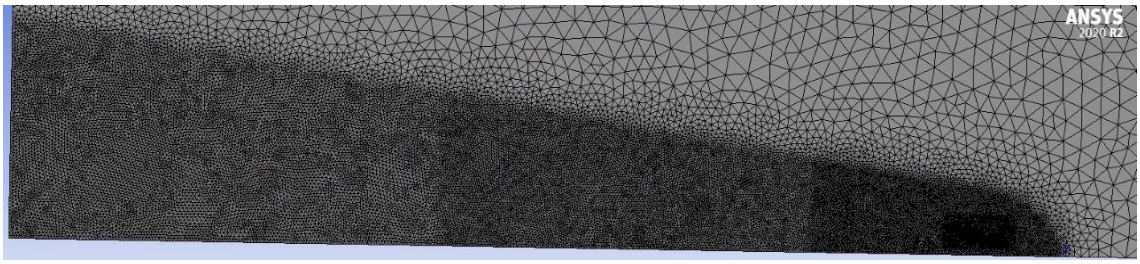

Figure 3-27. CFD Model Validation: CFD Case 1 wake mesh overview

Table 3-10. CFD Model Validation: CFD Case 1 mesh metrics

Mesh Metric	Average	Standard Deviation
Element Quality	0.73 (-18.9%)	0.25 (+25%)
Aspect Ratio	7.66 (-59.8%)	27.25 (-39.1%)
Skewness	0.25 (=)	0.13 (-13.3%)
Orthogonal Quality	0.75 (+1.4%)	0.14 (-12.5%)
Nº of elements	15.7e6 (+196%)	
Nº of nodes	3.4e6 (+100%)	

As observed in Figure 3-28, residuals reached pre-set values for convergence. Therefore, results were more reliable than baseline configuration with accuracy left to compare. As showed in the comparison of Figure 3-29 (visually) and Table 3-11 (analytically), CFD case 1 results are more accurate (closer to experimental results) than baseline configuration.

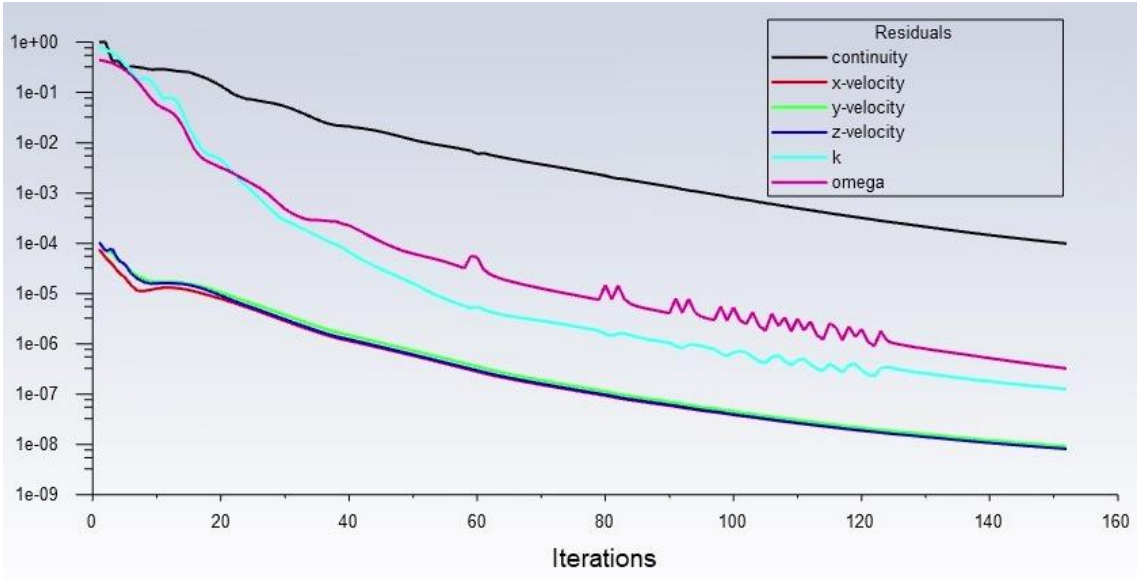

Figure 3-28. CFD Model Validation: CFD Case 1 residuals

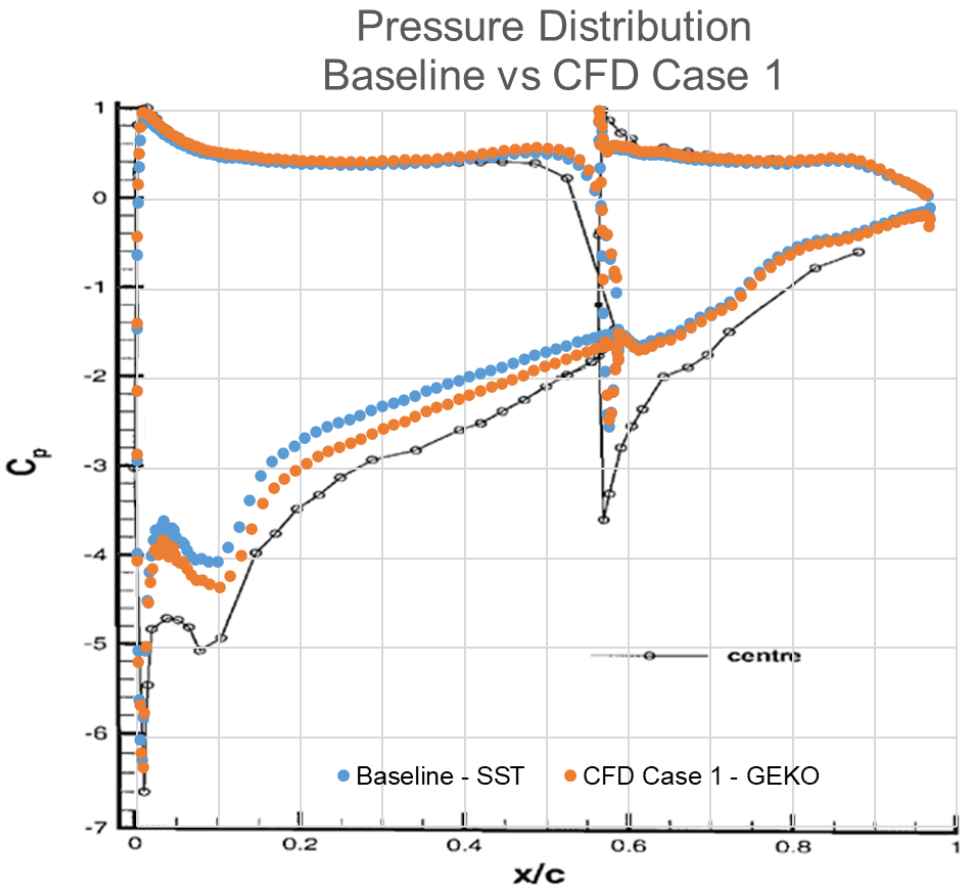

Figure 3-29. CFD Model Validation: CFD Case 1 pressure distribution (orange) compared to Baseline (blue) and experimental data from the literature (black) [3]

Table 3-11. CFD Model Validation: CFD Case 1 pressure distribution error compared to Baseline

Main Flap	Error [%]
Peak Suction	3.8 (-0.7)
Concave Minimum x/c 0.05	19.1 (-4.3)

3.2.3.4 Conclusions

Changes made improved convergence and accuracy of results, reducing the pressure distribution error between 0.7 and 4.3 %. Computation cost also increased as mesh elements increased by 196 %. While solution methods order was reduced from second to first to improve the convergence at the expense of accuracy, reversing this action would improve accuracy and the simulation may still converge. This would mean that fluid domain and mesh updates were the key reason for the convergence improvement.

3.2.4 CFD Case 2

3.2.4.1 Intent

Increase the accuracy of main flap pressure distribution calculation without deteriorating simulation convergence.

3.2.4.2 Changes made

Solution methods were changed to second order for pressure, momentum, turbulent kinetic energy and specific dissipation rate.

3.2.4.3 Results

As observed in Figure 3-30, residuals reached same values for convergence as in CFD Case 1. It did not stop automatically because values were pre-set to 1e-4 instead of 1e-3, just to check whether maximum number of iterations or simulation setup was the limitation to achieve lower residuals.

Simulation convergence is further confirmed by main flap Cl value evolution through the iterations, see Figure 3-31. Therefore, showed results were, at least, as reliable as CFD Case 1 with accuracy left to compare. Ans as showed in the comparison of Figure 3-32 (visually) and Table 3-12 (analytically), CFD Case 2 results were more accurate (closer to experimental results) than CFD Case 1 configuration.

It is important to highlight that the error in the peak suction does not necessarily mean that the simulation is wrong. Exists a physical limitation in the experiment where static pressure measurement points are concerned. Even if measurement point resolution was high in that area, it is still possible they missed the highest peak suction value.

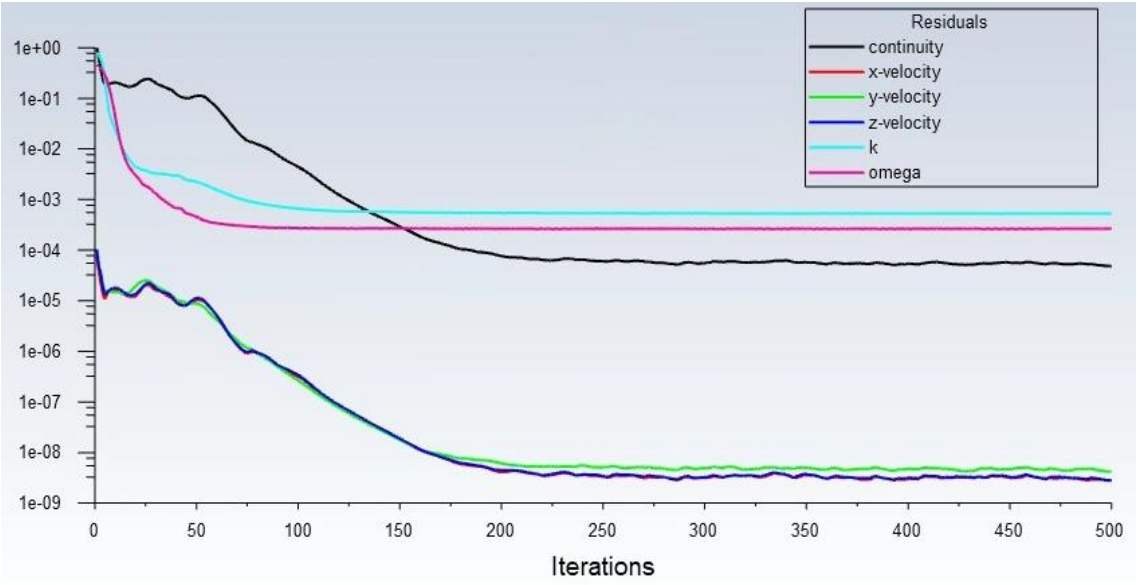

Figure 3-30. CFD Model Validation: CFD Case 2 residuals

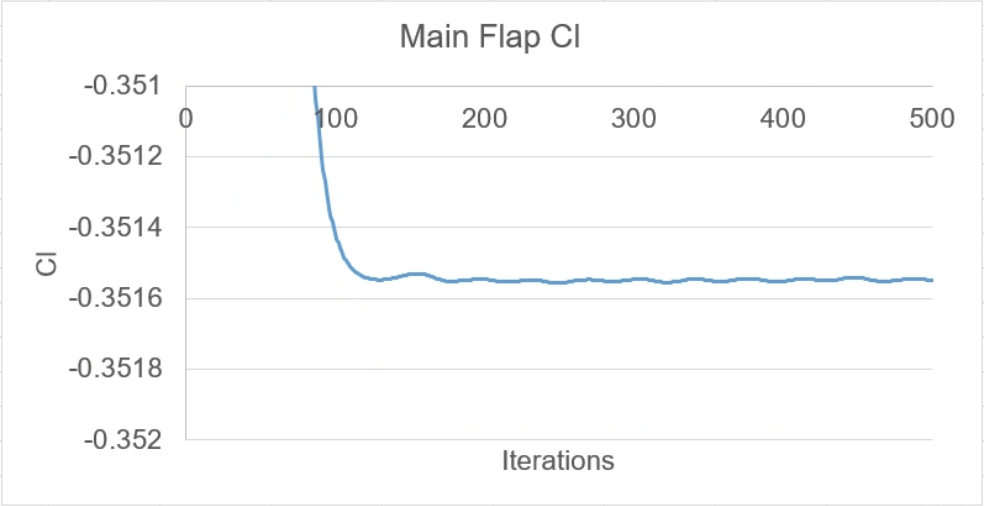

Figure 3-31. CFD Model Validation: CFD Case 2 main flap Cl convergence

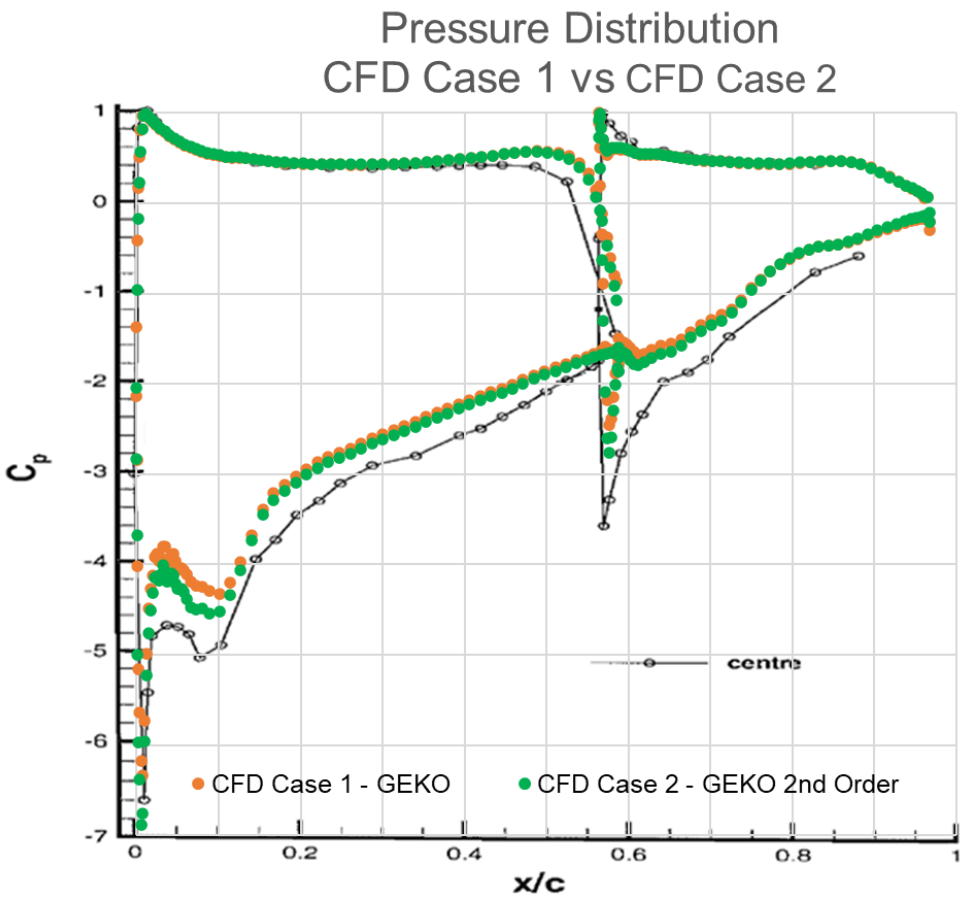

Figure 3-32. CFD Model Validation: CFD Case 2 pressure distribution (green) compared to CFD Case 1 (orange) and experimental data from the literature (black) [3]

Table 3-12. CFD Model Validation: CFD Case 1 pressure distribution error compared to Baseline

Main Flap	Error [%]
Peak Suction	4.5 (+0.7)
Concave Minimum x/c 0.05	14.9 (-4.2)

3.2.4.4 Conclusions

Accuracy of results were increased as error was generally reduced, reducing concave minimum (x/c) by 4.2 %. As previously mentioned, the error in the peak suction does not necessarily mean that it is a real error, most probably is a consequence of measurement resolution limitation from the experiment. The increase in accuracy was at the expense of increasing computational cost per iteration but achieving same level of residuals (1e-3) with almost same number of iterations (~150). Nevertheless, as simulations were run in Cranfield High Performance Computer cluster[1], CFD time was still short enough (~1.5 h) to not have a negative impact on the development of the thesis.

[1] Two Intel E5-2660 (Sandy Bridge) CPUs giving 16 CPU cores and 64GB of shared memory

3.2.5 Conclusions

CFD Case 2 setup provided best accuracy VMware Horizon computers could provide given their computational limitations. Different mesh strategies may have provided better accuracy, but a significant improvement was not likely to happen.

There were three main reasons not to have obtained better results: mesh resolution, turbulence model and uncertainty about the experiment. Regarding the last point, it has already been mentioned that the lack of resolution of measurement points in the peak suction may lead to discrepancies with simulation results. Regarding mesh resolution and turbulence model, if more powerful computers were available, further improvements of the model would have been undertaken:

- Mesh resolution:
    - Refining the gap between main flap TE and second flap LE.
    - Further flap surface and wake refinement would be recommended.
    - Reducing Boundary Layer stretching factor from 1.3 to 1.05.
- Turbulence model:
    - RANS GEKO is being used. Further investigation with more complex models such as DES (Detached Eddy Simulation) and LES (Large Eddy Simulation) would be recommended.

Therefore, based on CFD Case 2 model, next steps of the thesis were undertaken.

3.3 CFD Manual Deformations

This section is focused on 2D and 3D simulations to compare the effects of increasing main airfoil thickness and suction surface passive deformation. Besides, the difference in results between 2D and 3D is discussed.

3.3.1 2D Analysis

The objective of this analysis was to compare main airfoil baseline geometry (NACA 6408) against NACA 6412 and the hybrid NACA 6408-12 as in chapter 3.1.2.2 but this time using developed CFD model (chapter 3.2.4).

Same setup, including h/c ground clearance, as when developing the CFD model was used in order to keep flow characteristics as close as possible to [4] flow problem: double element wing, span length, flat and small endplate and h/c ground clearance. The only difference is that this was a 2D analysis, so 3D flow related complexity was avoided.

In Figure 3-33 change in aerodynamic KPI (Cl, Cd and -L/D) can be observed. From this analysis same conclusions as in chapter 3.1.2.2 are obtained. To avoid repetition, as summary, both downforce (Cl) and efficiency (-L/D) increased when increasing the main flap thickness; besides, suction surface deformation obtained performance close to the increase in thickness, producing same downforce but at the same time 1.4 % more drag, resulting into a 1.4% smaller efficiency compared to the increase in thickness.

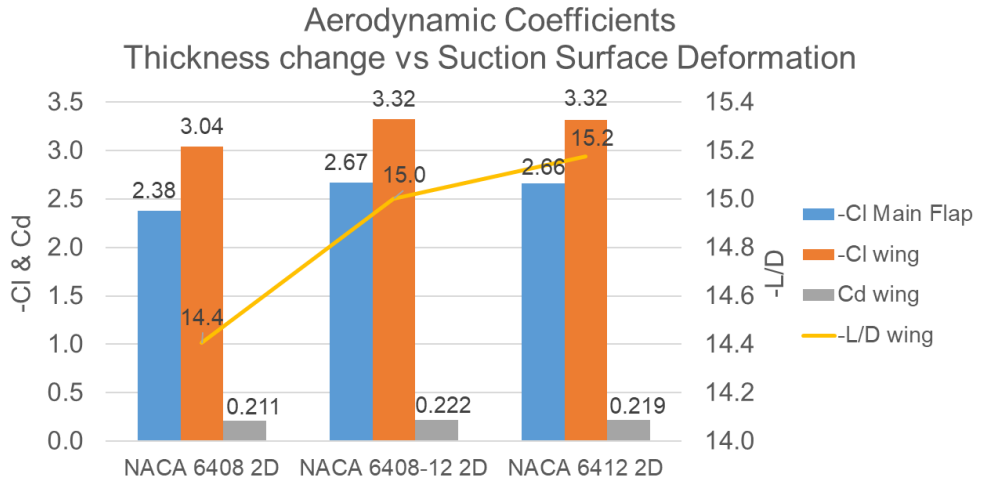

Figure 3-33. CFD Manual Deformations 2D: Double element wing aerodynamic coefficients change with thickness increase and suction surface deformation

3.3.2 3D Analysis

Once it was probed that airfoil suction surface would match increasing thickness KPI and even improve baseline geometry (initial thickness) values, 3D analysis was the next step. This analysis was necessary as in real life 3D effects exists and for low aspect ratio (span divided by chord length) wings (motorsport case) these are significant.

As explained in methodology, a range from 8% to 12% t/c thickness in steps of 1% was used for manual deformations. Observing Figure 3-34, pressure distribution changes when increasing manual deformation, reducing peak suction magnitude and increasing 0.1 – 0.25 x/c area values. This information was helpful to understand how deformation shape could change because of change in pressure distribution. Hence, useful in a later stage when thinking on an appropriate structural concept for the problem.

In Figure 3-35 the evolution of downforce and efficiency is showed. First, and most important as it is related to this thesis first objective, suction surface deformation match the performance of increasing airfoil thickness. Furthermore, it even has a slightly better performance (< 1% in downforce and efficiency) than NACA 6412 in this particular wing configuration. Second, increasing thickness or suction surface deformation does not increase performance (neither downforce nor efficiency) from baseline geometry (NACA 6408). However, a change in tendency is observed at NACA 6408-10, as from that point downforce (not efficiency) starts to increase again. This may indicate that higher deformations/thickness could provide an increase in downforce (compare to baseline) at the expense of reducing efficiency.

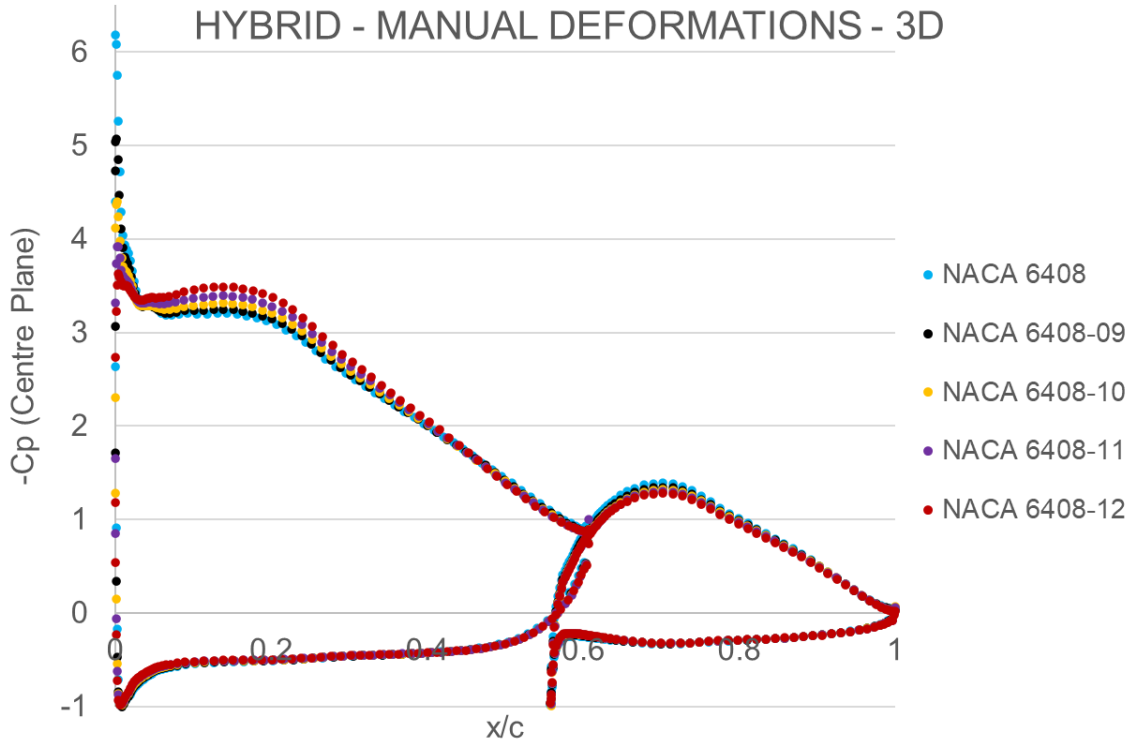

Figure 3-34. CFD Manual Deformations 3D: centre plane pressure distribution for different manual deformations (hybrid main flap)

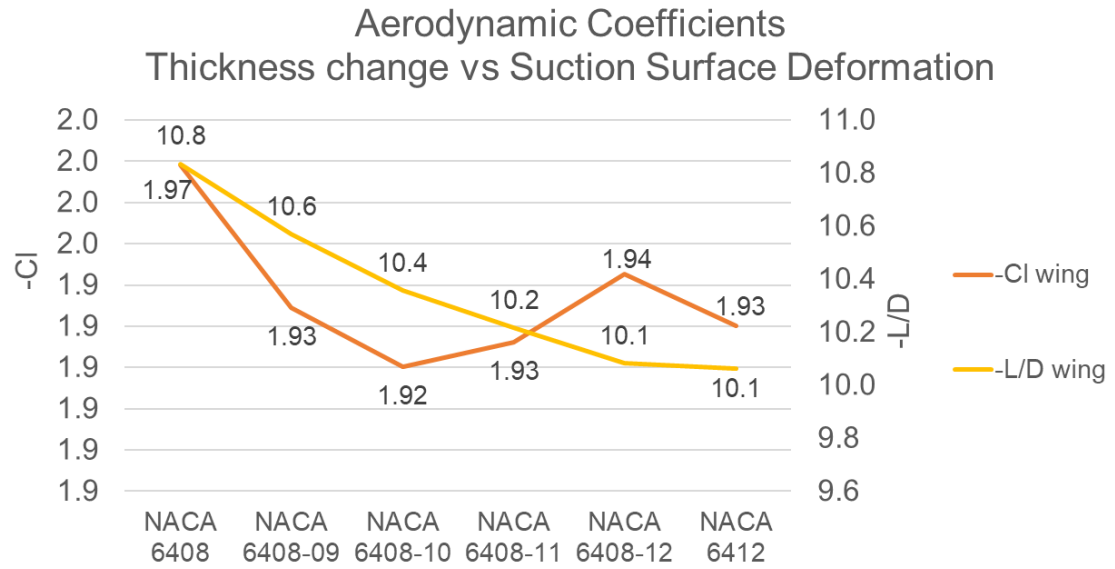

Figure 3-35. CFD Manual Deformations 3D: downforce and efficiency for different manual deformations (hybrid main flap)

3.3.3 2D vs 3D

In previous chapters it has been mentioned that 2D and 3D flow physics and therefore, flow field and results are different. In Figure 3-36 a pressure distribution comparison of those two different simulations for baseline (NACA 6408) and hybrid (NACA 6408-12) is shown.

First, this comparison highlighted the influence of 3D flow effects on wing performance where big pressure drop (absolute values) is observed in both flaps suction surface. Performance drop for KPI can be observed in Table 3-13.

Second, both in Figure 3-36 and Table 3-13 can be observed that the negative influence of the 3D effects was bigger when increasing thickness (remember that hybrid and thickness increase wing provided similar performance). It is logical as the suction surface gets closer to the end of the endplate as thickness/deformation increase.

This thesis focus has not been to provide a performance gain in 3D wings as that would require of geometry optimisation, hence more development time not possible to fit in the already busy project planning. Nevertheless, different ways to approach this optimisation are suggested in chapter 5.

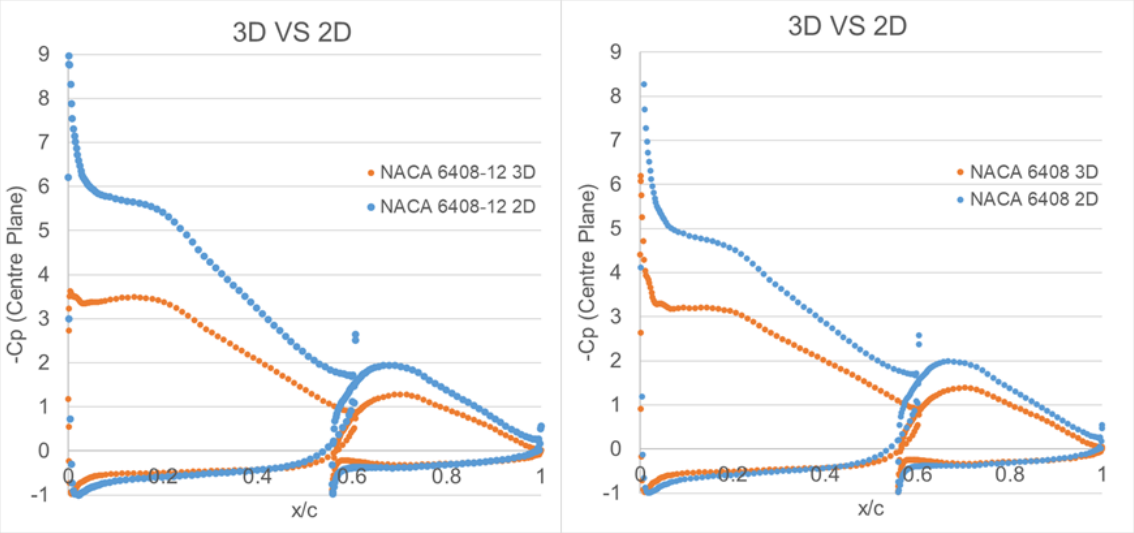

Figure 3-36. CFD Manual Deformations 2D vs 3D: pressure distribution comparison for 2D and 3D simulations (NACA 6408 left and NACA 6408-12 right)

Table 3-13. CFD Manual Deformations 2D vs 3D: Cl and -L/D comparison for 2D and 3D simulations

NACA 6408		Cl [-]	-L/D [-]
	2D	3.04	14.4
	3D	1.97 (-35.2%)	10.8 (-25%)
NACA 6408-12			
	2D	3.32	15.0
	3D	1.94 (-41.6%)	10.1 (-35.2%)

3.4 Fluid Structure Interaction

This section gives an answer to second and third objectives. Analysing if structural concepts could achieve required deformation and if exact deformations were not obtained, what would be the effect on aerodynamic KPI.

3.4.1 Structure Concept

Second objective of the thesis was to design most suitable structure to achieve desired deformation (hybrid airfoil NACA 6408-12). Hence, structural concepts were analysed to understand if they could provide desired deformation shape and magnitude. As the objective was not to optimise the structure, for a first approach a well-known material from ANSYS database was considered, structural steel, instead of composites as used in motorsport applications.

Focus was on suction surface deformation, therefore, to isolate results from other kind of deformations (bending and twisting), top surface was fixed.

3.4.1.1 Continuous Flap Surface

First, a simple approach of a continuous flap surface was taken. Shell elements were used which in this case, because of the low thickness (0.15 mm), it was necessary to avoid unaffordable 3 solid elements in thickness direction. One-way technique was used to import the CFD forces to static structural module, as explained in chapter 1.2.4.

However, as shown in Figure 3-37, the obtained deformation shape is far from the objective. There were two main issues: stiffness distribution combined with pressure distribution, and LE and TE degrees of freedom.

On one side, LE had higher stiffness than the TE, for a constant thickness surface, because of the LE curved section inertia. Besides, pressure and target deformation distribution, as showed in previous chapters, is not constant. Therefore, further optimisation would be required to balance those conditions and requirements.

On the other side, top surface was modelled as infinitely rigid, and TE and LE were rigid connections between top and bottom surfaces. This combined with a stiffness distribution concentrated in the LE area, generated internal moments with changes in sign provoked LE area to deform to the inside of the structure while the mid-TE area deformed to the outside. Change in moments sign can be appreciated in Figure 3-38 as low stress areas were a result of zero or very low moments.

Even if stiffness distribution was changed, a part of the surface would still have deformed to the inside instead of the outside of the flap. Hence, this concept was concluded not to be able to provide the desired deformation.

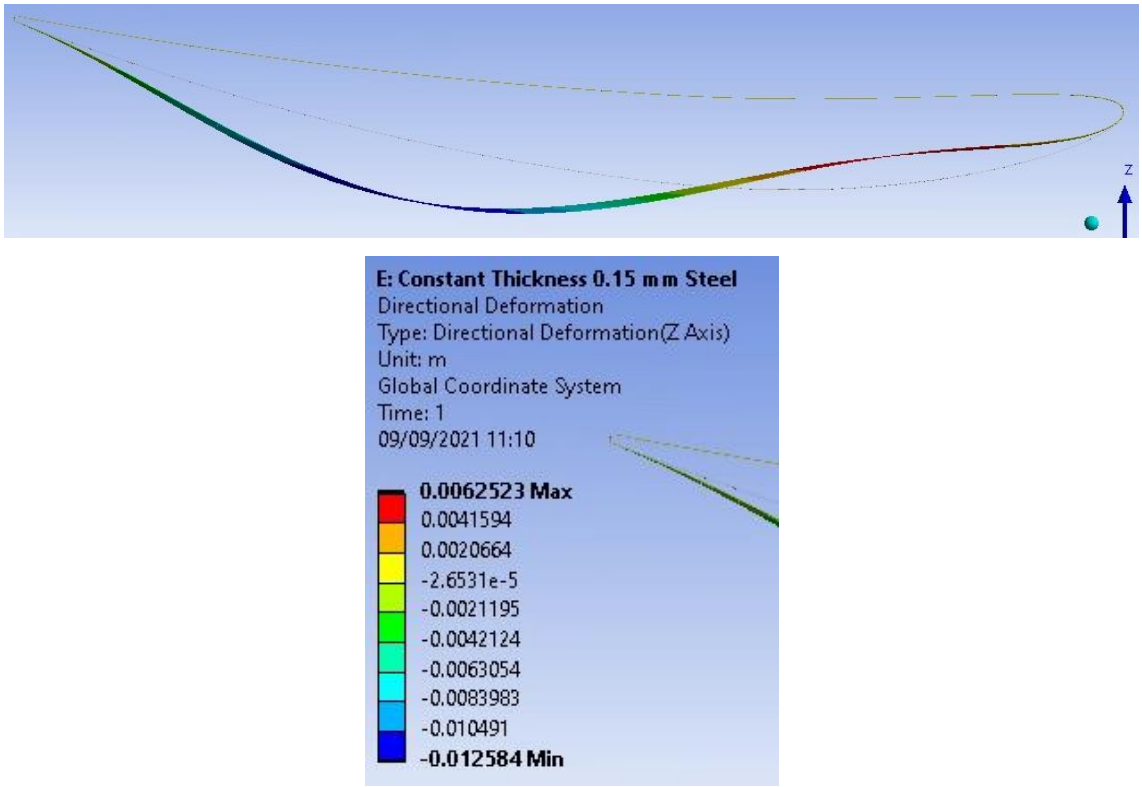

Figure 3-37. FSI Structural Modelling: Continuous flap surface deformation Z axis

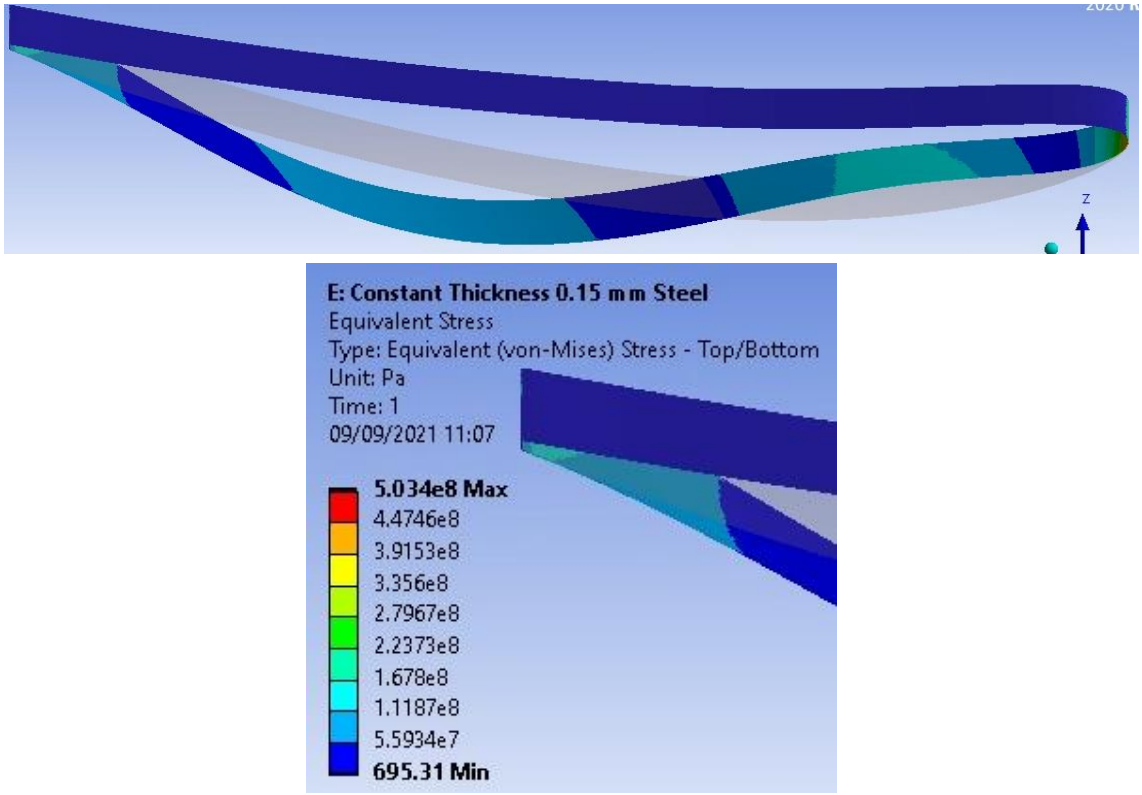

Figure 3-38. FSI Structural Modelling: Continuous flap surface Von-Mises Stress

3.4.1.2 Discontinuous Flap Surface

As a response to changes in internal moments sign, it was decided to split the suction surface in 3 surfaces: LE, spring and TE surfaces. This meant that the flap was made of two physically independent surfaces: spring surface (green and orange in Figure 3-39) and the rest.

In Figure 3-39, structure concept modelling strategy is visually represented. As previously mentioned, top surface was fixed (blue) to isolate suction surface deformation from other type of deformations. Then, spring surface was overlapped with surfaces from LE and TE in the orange highlighted area. The overlap was modelled so that in plane surface sliding was allowed but not surface normal relative displacements. Green surface was constrained so that only in-plane (same as figure plane view) displacement was allowed. Finally, a spring connection was modelled between top and spring surfaces to counteract the aerodynamic forces and limit the deformation of the structure.

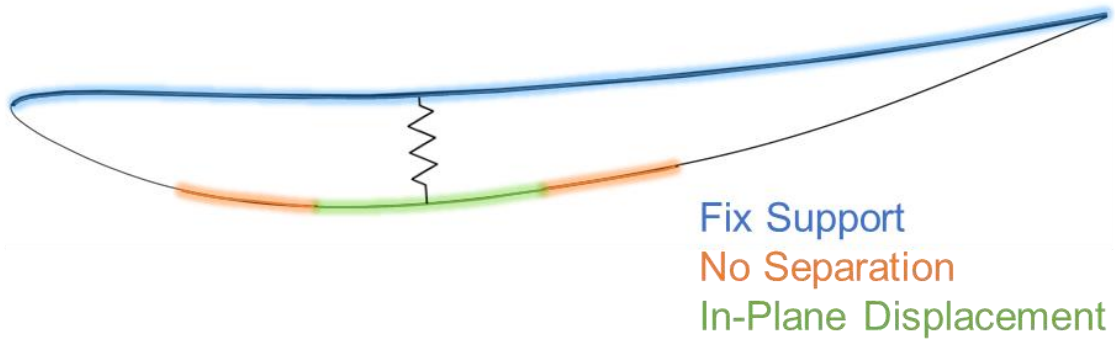

Figure 3-39. FSI Structural Modelling: Discontinuous flap surface concept model

Figure 3-40 shows this structural concept deformation and the outcome was positive. First, the whole surface deformed to the outside of the flap. Second, the deformation magnitude was close to the targeted deformation shown in Figure 3-41. Furthermore, the deformation was easy to adjust by adjusting spring stiffness and surfaces thickness, see Table 3-14.

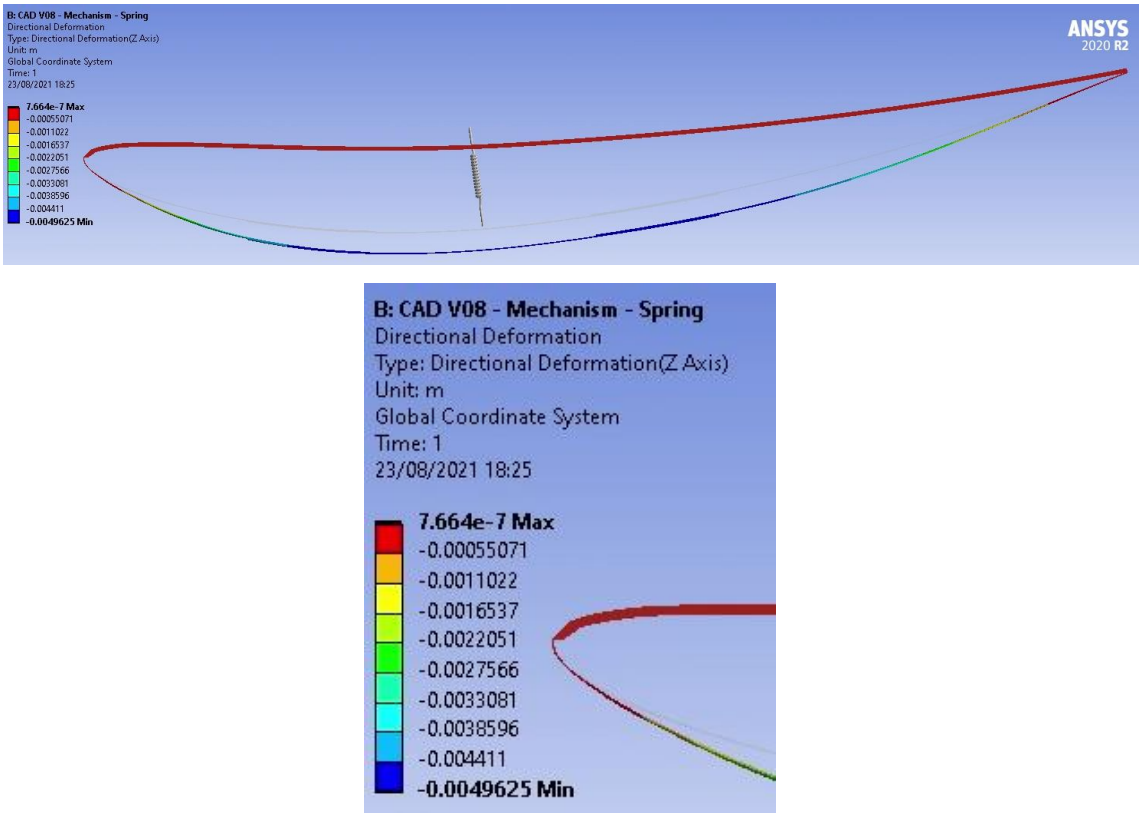

Figure 3-40. FSI Structural Modelling: Discontinuous flap surface deformation Z axis

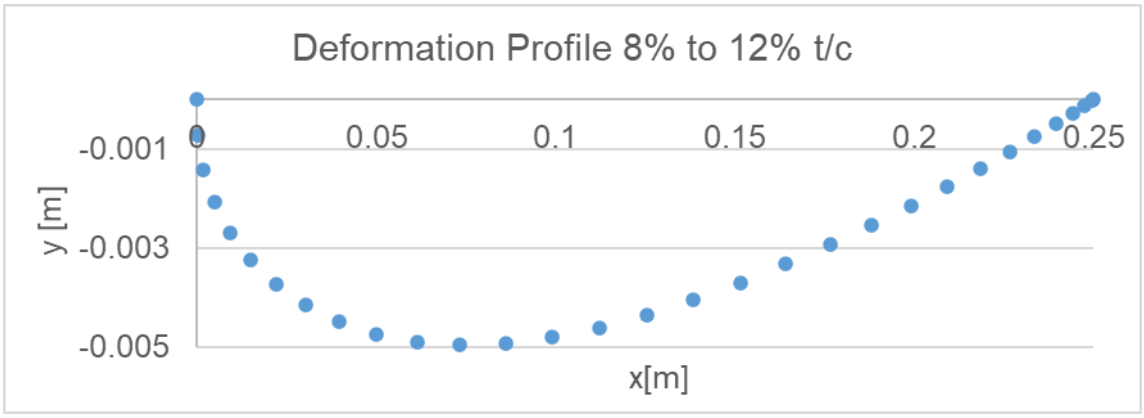

Figure 3-41. Target deformation to achieve NACA 6408-12 from NACA 6408

Table 3-14. FSI Structural Modelling: Discontinuous flap surface parameters

	Thickness [mm]	Stiffness [kN/m]
LE Surface	0.2	-
Spring Surface	0.3	-
TE Surface	0.3	-
Spring	-	16

In Figure 3-42 a comparison between target deformation profile (NACA 6408-12) and obtained real deformation is showed. As it can be observed, there is a difference at x 0.02 and 0.17 [m] which could be partially solved by tunning surface thickness. However, LE difference is not possible to solve completely because of the proximity to the stagnation point and therefore, positive pressure acting against the target deformation.

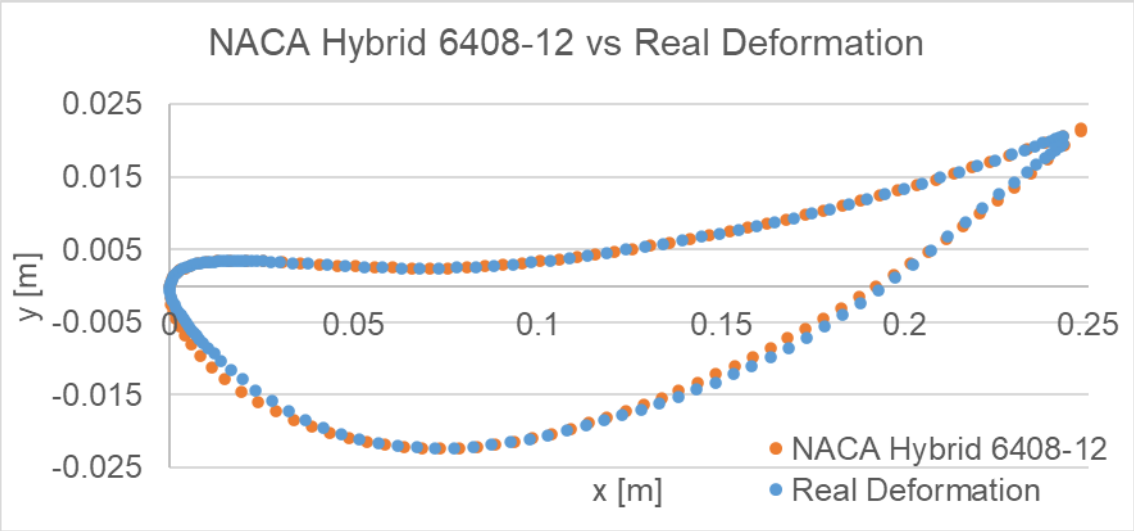

Figure 3-42. FSI Structural Modelling: target profile against obtained deformation

It is important to highlight that deformation results had an error. Due to some issues when using shell elements, solid elements were finally used. As stated before, this was an issue as when using solids, 3 elements are needed in the thickness direction to correctly calculate the bending stiffness. Although that is the requirement, only one element was meshed as 3 would have been unaffordable from the computational cost point of view.

Moreover, the modelling strategy of the structure should be revised once a version to manufacture is defined.

3.4.2 Effects on Aerodynamic Performance

Third objective of the thesis was to study the effects of deformation profile deviations on aerodynamic key performance indicators. For this reason, obtained deformation profile from first one-way FSI simulation was exported to modify the CAD and run again a CFD analysis.

Results represented in Figure 3-43 showed that the obtained real deformation produced 4.6% less downforce and 1% less efficiency, therefore 3.6% less drag, than target deformation. Hence, in this case, real deformation did not increase downforce but decreased drag at the expense of 1% efficiency.

A second static structural simulation was done by using the updated CFD forces. Deformation remained practically the same; hence, in this case, not having used a computationally much more expensive method as 2-way FSI did not induce significant uncertainties.

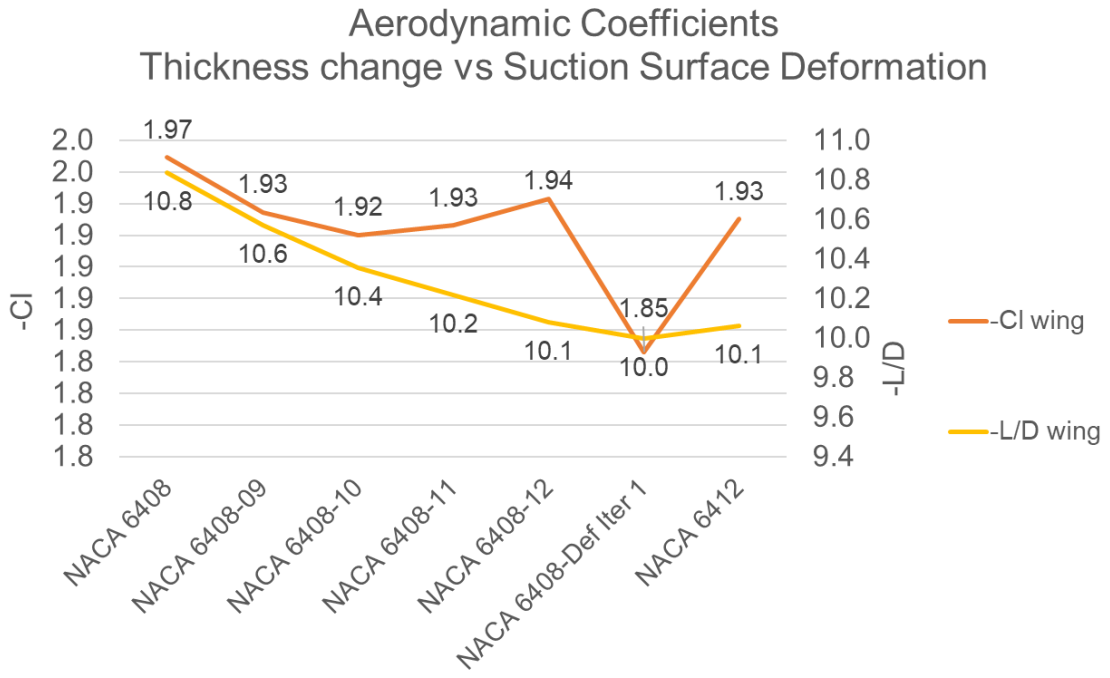

Figure 3-43. FSI Effects on Aerodynamic Performance: real deformation KPI

3.4.3 Effects on Deformation Limitation

At the beginning of the project, as using a flap continuous surface was the first idea, CFD manual deformation analysis was limited by strain values to a range from 8% to 12% t/c. However, with the discontinuous flap surface concept, it was possible to aim for higher deformations which could be interesting as highlighted in chapter 3.3.2.

Therefore, 16% and 20% t/c manual deformations were simulated and in Figure 3-44 obtained results are shown. As suspected in chapter 3.3.2, higher levels of deformation provided more downforce than baseline geometry (NACA 6408) in exchange of further efficiency decrease. Besides, Figure 3-45 confirmed the tendency of pressure distribution change when increasing deformation.

Further investigation would be necessary to determine whether the structure concept could achieve those deformations and the effects of real deformations on performance.

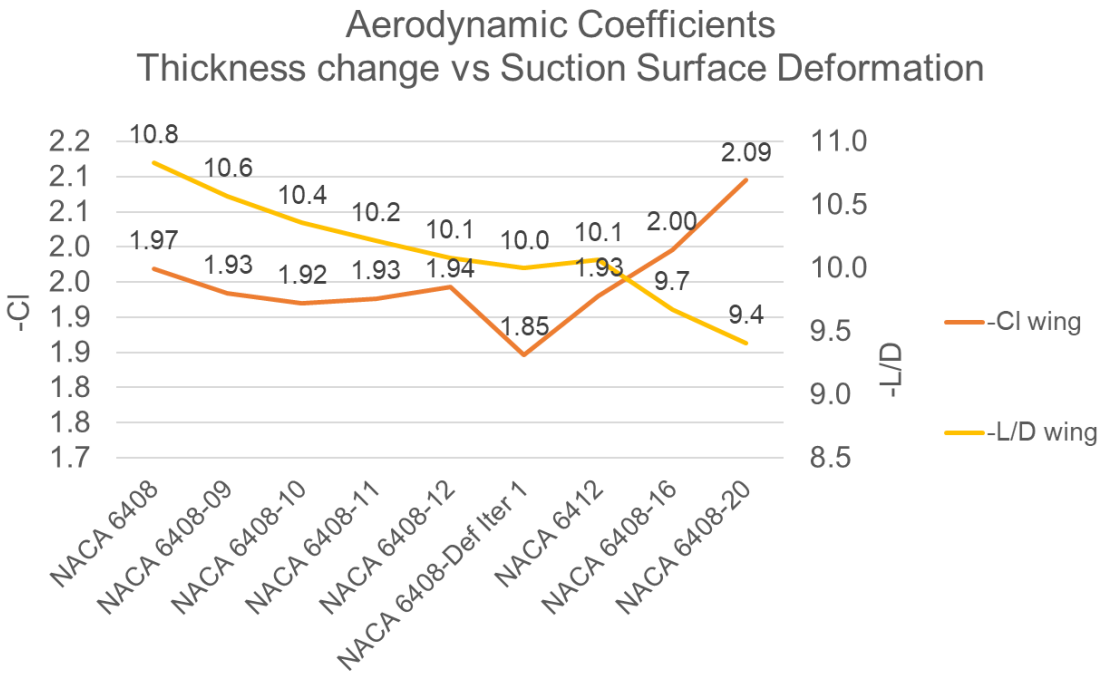

Figure 3-44. FSI Effects on Deformation Limitation: high deformations KPI

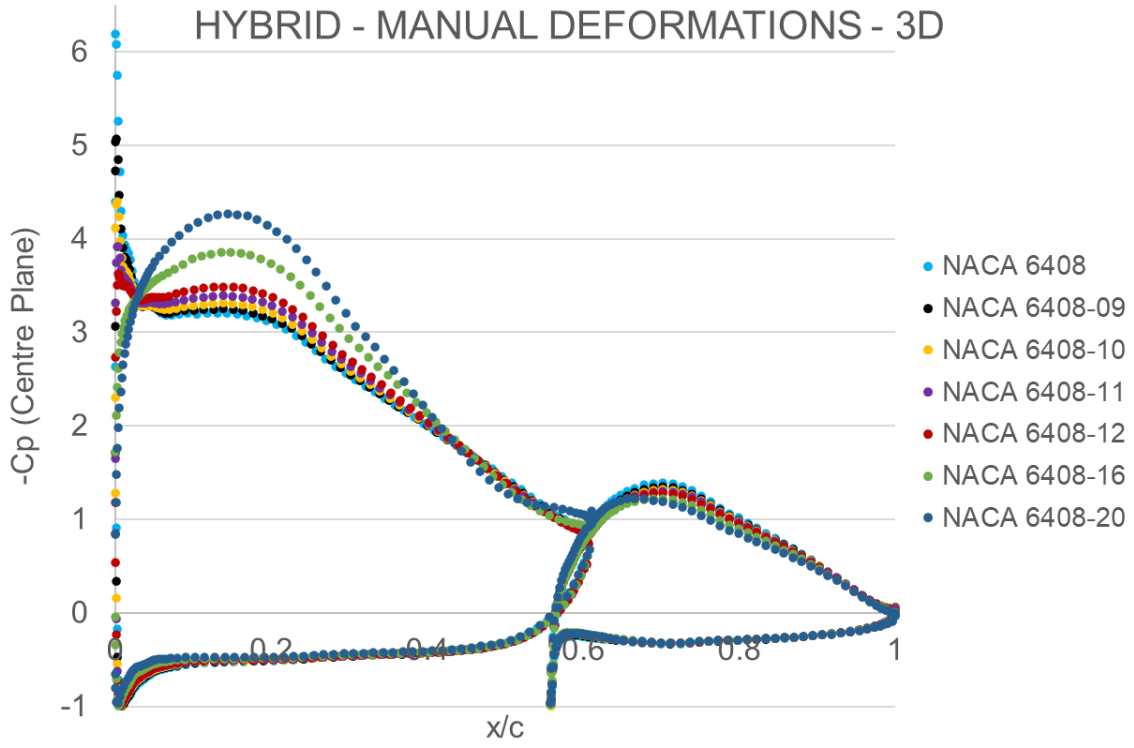

Figure 3-45. FSI Effects on Deformation Limitation: centre plane pressure distribution for different manual deformations (hybrid main flap)

4 CONCLUSIONS

This thesis has demonstrated that passive deformation of suction surface match the effects of increasing airfoil thickness within a 1% margin. Limited by time restrictions, this thesis has been focused on comparing deformation and thickness increase in 2D and 3D flow for a given ground clearance and in straight-line conditions. Besides, two structural concepts were analysed to determine which could achieve target deformation. Therefore, this thesis has been focused on the conceptual design of a new passive airfoil morphing. Further investigations to complete the study of this novel aero-structural concept are recommended in chapter 5.

At early stages of the project, it was deemed that a single airfoil was too sensitive to the increase of APG due to ground effect and therefore not suitable for the development of this project. For this reason, a two double element wing approach was analysed and considered appropriate for further study.

During the CFD model validation process, k-ω SST and GEKO (default values) turbulence models have obtained best convergence and accuracy for the given mesh setup. Finally, a pressure distribution accuracy in between 86% and 93% has been obtained for the main flap suction surface. Although different mesh strategies could have provided better accuracy, a significant improvement was not likely to happen. After all, VMware Horizon computer has been the major limitation for further improvement of the CFD model.

Based on validated CFD model, it has been demonstrated that for the given double element wing, in 2D CFD analysis, both downforce (Cl) and efficiency (-L/D) increases when increasing the main flap thickness; besides, suction surface deformation obtained performance has been close to the increase in thickness, producing same downforce but at the same time 1.4 % more drag, resulting into a 1.4% smaller efficiency.

The 3D CFD analysis performed in this thesis has demonstrated that 3D effects, and therefore losses compared to 2D KPI, increase when increasing airfoil thickness or suction surface deformation. As a result, advantages showed in the

2D analysis were reduced or even dismissed. However, it has also been probed that high level of deformation (16% and 20% t/c) could compensate losses achieving higher downforce (+6.1%) than baseline geometry (NACA 6408) at the expense of efficiency decrease (-13%).

Finally, two different structure concepts have been analysed. On the one hand, flap continuous surface did not provide the required deformation because of internal moments sign variation along the suction surface. Besides, this concept limited maximum deformation depending on material maximum elastic strain. On the other hand, discontinuous flap surface has been demonstrated to be able to provide a deformation close to the target. Moreover, the effects of deformation profile deviation (compared to target) were quantified as a loss of 4.6% in downforce and 1% in efficiency. Besides, this structural concept did not have the strain limitation of the previous one, being able to achieve higher deformations (16% and 20% t/c) and therefore, as probed in with CFD manual deformations, higher downforce.

5 FUTURE WORK

As commented in conclusions this thesis has been focused on the conceptual design of a novel passive airfoil morphing concept. Therefore, a wide range of possibilities as future work are available. To make it easier to identify, suggestions are split into different categories.

5.1 CFD Model Accuracy

There are three main reasons not to have obtained better results: mesh resolution, turbulence model and uncertainty about the experiment. Regarding the last point, it has already been mentioned than the lack of resolution of measurement points in the peak suction may lead to discrepancies with simulation results. Regarding mesh resolution and turbulence model, if more powerful computers were available further improvements of the model would be undertaken:

- Mesh resolution:
  - Refining the gap between main flap TE and second flap LE.
  - Further flap surface and wake refinement would be recommended.
  - Reducing Boundary Layer stretching factor from 1.3 to 1.05.
- Turbulence model:
  - RANS GEKO is being used. Further investigation with more complex models such as DES (Detached Eddy Simulation) and LES (Large Eddy Simulation) would be recommended.
- Experiment:
  - Analyse the accuracy of the CFD model running an experiment with the developed geometry.

5.2 Structural Model Accuracy

The use of shell elements is more appropriate for this geometry given the low thickness of the wing. Besides, the use of no-separation contact in the overlap could induce an error compared to reality depending on the actual design to manufacture and test.

5.3 Fluid Structure Interaction

The potential of fluid structure simulations has not been fully used. For example, a 2-way FSI analysis with a transient CFD simulation could be run to simulate an acceleration in straight-line. This analysis would help to understand the effects of this morphing concept in the aero balance of the car, the effects on off-body flow and elements downstream the front wing, for example. Moreover, considering added mass-effect on the structure would be interesting when designing the structure to manufacture.

5.4 Geometry Optimisation

A single/multi-objective optimisation tool could be used or developed so that the deformation of suction surface and/or size of the endplate could be optimised to achieve best downforce or efficiency or both for instance. This thesis has been focused on achieving a deformation close to the increase in thickness, but that does not mean other kind of deformation would not be better.

5.5 Effects of Car States (Yaw, Roll, Pitch, Heave)

This thesis has been focused on the analysis of straight-line condition for a given ground clearance. However, for better understanding of the integration of this morphing concept into a car, it would be convenient to analyse its behaviour under different car states: yaw, roll, pitch and heave. Generally, this short of analysis is recommended to be done in a wind tunnel and not in CFD, as wind tunnel is much faster and versatile for this type of analysis.

5.6 Morphing Concept Applied to other Geometries

Analyse this principle in other elements, for example, the underbody of the car. It would be interesting to analyse, for instance, the effects it would have if applied on the smallest section of the new 2022 Formula One Cars Venturi tunnels.

5.7 Passive or Active Morphing

This concept could also be developed into an active system. Indeed, it would be helpful to compensate positive pressure conditioned areas such as the LE.

REFERENCES

[1] Fédération Internationale de l'Automobile (FIA), "2021 FORMULA 1 TECHNICAL REGULATIONS," 2020.

[2] J. Katz, "Race Car Aerodynamics Designing for Speed," Bentley Publishers, 1995.

[3] "Airfoil Tools," [Online]. Available: http://airfoiltools.com/. [Accessed 06 2021].

[4] J. D. C. Zerihan, An Investigation into the Aerodynamics of Wings in Ground Effect (Ph.D. Thesis), University of Southampton, 2001.

[5] R. L. Bisplinghoff, H. Ashley and R. L. Halfman, Aeroelasticity, Mineola, New York: Dover Publications, Inc., 1995.

[6] Livermore Software Technology, ICFD Theory Manual, 2014.

[7] "Wikipedia," [Online]. Available: https://en.wikipedia.org/wiki/Grumman_X-29#cite_note-FOOTNOTEPamadi2004-6. [Accessed 08 2021].

[8] "NASA," [Online]. Available: https://www.nasa.gov/centers/armstrong/history/experimental_aircraft/x-29.html. [Accessed 08 2021].

[9] R. Giuliana, "F1 Only.fr," 15 06 2021. [Online]. Available: https://f1only.fr/ailerons-flexibles-f1-news-15-juin/. [Accessed 08 2021].

[10] "Sporting Blogs," [Online]. Available: https://sportingblogs.wordpress.com/2011/04/15/red-bull-gives-you-flexible-front-wings/a-comparison-of-red-bull-and-mclarens-2011-front-wings-with-red-bulls-front-wing-clearly-flexing-more-than-their-rivals/. [Accessed 08 2021].

[11] Z. Goraj, “An Overview of the De-Icing and Anti-icing Technologies with Prospects for the Future,” *ICAS,* 2004.

[12] M. Bashir, S. Longtin-Martel, R. Mihaela Botez and T. Wong, “Aerodynamic Design Optimization of a Morphing Leading Edge and Trailing Edge Airfoil–Application on the UAS-S45,” *MDPI,* vol. 11, no. 1664, 2021.

[13] “The Formula 1 Wiki,” [Online]. Available: https://f1.fandom.com/wiki/Drag_Reduction_System. [Accessed 08 2021].

[14] M. Hepperle, “JavaFoil,” [Online]. Available: https://www.mh-aerotools.de/airfoils/javafoil.htm.

[15] ANSYS, Fluent 2020 R2 User's Guide, 2020.

APPENDICES

Appendix A CAD for CFD Model Validation

In order to validate the CFD model with experimental results from [4], analysed geometry CAD model was obtained, see the following tables.

Main Element Coordinates			
Suction Surface		Pressure surface	
x/c	y/c	x/c	y/c
0	0	0	0
0.0006	-0.0044	0.0006	0.0047
0.0011	-0.0063	0.0012	0.0064
0.0029	-0.0098	0.003	0.0102
0.0058	-0.0134	0.0059	0.0136
0.0087	-0.0156	0.0089	0.0159
0.0117	-0.0173	0.0118	0.0176
0.0146	-0.0188	0.0148	0.0184
0.0175	-0.0203	0.0177	0.0189
0.0205	-0.0217	0.0207	0.0194
0.0234	-0.0231	0.0236	0.0199
0.0263	-0.0245	0.0265	0.0204
0.0293	-0.0258	0.0295	0.0208
0.0322	-0.027	0.0324	0.0212
0.0351	-0.0283	0.0354	0.0217
0.041	-0.0306	0.0412	0.0225
0.0469	-0.0328	0.0471	0.0232
0.0528	-0.0348	0.053	0.0239
0.0586	-0.0366	0.0589	0.0245
0.0704	-0.0398	0.0707	0.0256
0.0821	-0.0422	0.0824	0.0265
0.0939	-0.0441	0.0942	0.0272
0.1056	-0.0452	0.1059	0.0278
0.1174	-0.0457	0.1177	0.0282
0.1468	-0.0448	0.1471	0.0293
0.1762	-0.043	0.1765	0.0303
0.2056	-0.0407	0.2059	0.031
0.235	-0.0379	0.2353	0.0314
0.2644	-0.0347	0.2647	0.0316
0.2938	-0.0309	0.2941	0.0315
0.3232	-0.0267	0.3234	0.0311
0.3526	-0.0219	0.3528	0.0305

0.382	-0.0167	0.3822	0.0295
0.4114	-0.011	0.4116	0.0283
0.4409	-0.0049	0.441	0.0268
0.4703	0.0018	0.4704	0.0257
0.4997	0.009	0.4998	0.0261
0.5291	0.0166	0.5292	0.0282
0.5409	0.0198	0.5409	0.0295
0.5527	0.023	0.5527	0.0311
0.5644	0.0264	0.5645	0.033
0.5762	0.0298	0.5762	0.0352
0.5821	0.0316	0.5821	0.0364
0.588	0.0333	0.588	0.0377

Flap Coordinates Reference Incidence of 14.1º			
Suction Surface		Pressure surface	
x/c	y/c	x/c	y/c
0.5643	0.0757	0.5643	0.0757
0.5687	0.0633	0.572	0.0863
0.5744	0.0601	0.5785	0.0886
0.5805	0.0597	0.5849	0.0908
0.5868	0.0605	0.5914	0.0929
0.5931	0.0614	0.5979	0.0951
0.6248	0.0678	0.6302	0.1059
0.657	0.0779	0.6625	0.1167
0.6896	0.0908	0.6948	0.1275
0.724	0.1065	0.7271	0.1383
0.7573	0.1249	0.7594	0.1491
0.7895	0.1434	0.7918	0.16
0.8229	0.1617	0.8241	0.1709
0.8566	0.1789	0.8567	0.1836
0.8895	0.1967	0.8897	0.1996
0.923	0.2158	0.9232	0.2186
0.9564	0.2345	0.9567	0.2372
0.9669	0.2402	0.967	0.2429